

SEISMIC BEHAVIOR AND DESIGN OF URBAN
AREA TUNNEL LININGS*

A Final Project Report Submitted to National Science
Foundation for NSF Award Number PFR-7822879 under NSF
Program, Entitled "Research Initiation in Earthquake
Hazards Mitigation,"

by

Subhash C. Anand, Principal Investigator
Department of Civil Engineering
Clemson University
Clemson, S.C. 29631

January, 1982

* Any opinions, findings, and conclusions or recommendations
expressed in this publication are those of the author, and
do not necessarily reflect the views of the National Science
Foundation.

ABSTRACT

Recent observations indicate that underground lifelines have received heavy damage due to the occurrence of earthquakes in their vicinity. Because of the importance of these lifelines to the safety and health of the people at the time of the disaster, their capacity to survive an earthquake is vitally important. The research described in this investigation attempts to ascertain the influence of superimposed concentrated (or line) footing loads of buildings on shallow buried rigid pipes in urban areas in the event of an earthquake.

As no information currently exists in the literature concerning the transfer of static concentrated (or line) footing loads on underground concrete pipes, static analyses using the finite element technique are initially performed for various loading conditions. Because of the insignificant influence of nonlinear material properties on load calculations for buried pipes, as demonstrated by other investigators, only linear elastic material properties are assumed in the static analyses. Dynamic analyses are performed on the finite element model of the system using linear as well as nonlinear soil properties. The latter is achieved by a combination of the equivalent linear method and the method of complex response with complex moduli.

The response of the pipe-soil system subjected to an earthquake base motion is calculated to yield the time histories of the vertical and horizontal displacements of the pipe. The finite element model of the pipe alone is then subjected to these displacements at specific times to yield the normal stresses in the outer and inner fibers of the

pipe due to seismic loads. Addition of these stresses to the corresponding static stresses leads to total stresses for which buried pipes in urban areas in seismic zones must be designed.

Maximum stresses and dynamic load factors for various loading conditions are calculated and presented. It is seen that the additional stresses due to an earthquake with a maximum acceleration of 0.15g may be as high as 180% of those due to the gravity loads for some soils and loading conditions. Estimates are made concerning the magnitudes of total stresses that can occur in shallow buried rigid pipes in the event of an earthquake. Recommendations for future research for a better assessment of pipe stresses are also made.

TABLE OF CONTENTS

	Page
TITLE PAGE	i
ABSTRACT	ii
ACKNOWLEDGEMENTS	iv
LIST OF TABLES	vii
LIST OF FIGURES	vii
INTRODUCTION	1
Related Research	5
DETERMINATION OF PIPE STRESSES	8
Static Analysis	9
Loading, Geometry, and Material Properties	9
Finite Element Model	11
Dynamic Analysis	16
LUSH - Theory and Description	17
Method of Complex Response	18
The Discrete Fourier Transform	19
The Equivalent Linear Method	22
Program Description	23
Development of Finite Element Model for Dynamic Analysis	28
Selection of Model Dimensions and Boundary Conditions	28
Input Motion	31
Maximum Frequency	32
Interpolation Control	32
Mass Matrix	34
Material Properties	34
Iterations on Soil Properties	35
Solution Procedure	35
EVALUATION OF PIPE STRESSES	39
General Considerations	39
Nomenclature and Sign Convention	40
Maximum Stresses and Dynamic Load Factors	41
Effect of Variable Load Width on Pipe Stresses	70
Strain-Independent Soil Properties	70
Strain-Compatible Soil Properties	77

Table of Contents (Cont'd)

	Page
Comparison of Stresses due to Strain-Independent and Strain Compatible Soil Properties	80
Medium Soil	80
Hard Soil	81
Effect of Soil Stiffness on Pipe Stresses	82
Strain-Independent Soil Properties	82
Strain-Compatible Soil Properties	83
CONCLUSIONS AND SUGGESTIONS FOR FUTURE RESEARCH	
Conclusions	84
Suggestions for Future Research	86
LIST OF REFERENCES	89

Preceding page blank

LIST OF TABLES

Table	Page
1. Load Cases Analyzed for Static and Dynamic Analyses	10
2. Strain-Compatible Soil Properties	24
3. Non-dimensional Tangential Stresses in Pipe for Various Load Cases	71
4. Non-dimensional Maximum Static and Total Stresses, and Dynamic Load Factors (DLF) for Various Load Cases	73

LIST OF FIGURES

Figure	Page
1. Underground Tunnel or Pipe	4
2. Tunnel Lining or Pipe and Superimposed Surface Load	4
3. Geometry of the Region Included in the Finite Element Analysis	13
4. Finite Element Mesh	14
5. Finite Element Mesh of the Pipe	15
6. Strain-Compatible Shear Modulus Reduction Factor	25
7. Strain-Compatible Critical Damping Ratio	26
8. Boundary Conditions Used for Horizontal and Vertical Excitations	30
9. Earthquake Acceleration Time History	33
10. Typical Displacement Time History at Point A Due to Horizontal Excitation	37

List of Figures (Cont'd)

Figure	Page
11. Typical Displacement Time History at Point A Due to Vertical Excitation	39
12. Total Stresses at the Outer Face of the Pipe for the Load Case M-0-I for Horizontal and Vertical Accelerations at 0.64 Sec.	42
13. Total Stresses at the Inner Face of the Pipe for the Load Case M-0-I for Horizontal and Vertical Accelerations at 0.64 Sec.	43
14. Total Stresses at the Outer Face of the Pipe for the Load Case M-0-D for Horizontal and Vertical Accelerations at 1.12 and 0.64 Sec., Respectively	44
15. Total Stresses at the Inner Face of the Pipe for the Load Case M-0-D for Horizontal and Vertical Accelerations at 1.12 and 0.64 Sec., Respectively	45
16. Total Stresses at the Outer Face of the Pipe for the Load Case M-d-I for Horizontal and Vertical Accelerations at 0.64 Sec.	46
17. Total Stresses at the Inner Face of the Pipe for the Load Case M-d-I for Horizontal and Vertical Accelerations at 0.64 Sec.	47
18. Total Stresses at the Outer Face of the Pipe for the Load Case M-d-D for Horizontal and Vertical Accelerations at 1.28 and 1.12 Sec., Respectively	48
19. Total Stresses at the Inner Face of the Pipe for the Load Case M-d-D for Horizontal and Vertical Accelerations at 1.28 and 1.12 Sec., Respectively	49
20. Total Stresses at the Outer Face of the Pipe for the Load Case M-2d-I for Horizontal and Vertical Accelerations at 1.04 and 0.64 Sec., Respectively	50
21. Total Stresses at the Inner Face of the Pipe for the Load Case M-2d-I for Horizontal and Vertical Accelerations at 1.04 and 0.64 Sec., Respectively	51
22. Total Stresses at the Outer Face of the Pipe for the Load Case M-2d-D for Horizontal and Vertical Accelerations at 1.28 and 1.12 Sec., Respectively	52

List of Figures (Cont'd)

Figure	Page
23. Total Stresses at the Inner Face of the Pipe for the Load Case M-2d-D for Horizontal and Vertical Accelerations at 1.28 and 1.12 Sec., Respectively	53
24. Total Stresses at the Outer Face of the Pipe for the Load Case M-4d-I for Horizontal and Vertical Accelerations at 1.12 and 0.72 Sec., Respectively	54
25. Total Stresses at the Inner Face of the Pipe for the Load Case M-4d-I for Horizontal and Vertical Accelerations at 1.12 and 0.72 Sec., Respectively	55
26. Total Stresses at the Outer Face of the Pipe for the Load Case M-4d-D for Horizontal and Vertical Accelerations at 0.96 and 1.28 Sec., Respectively	56
27. Total Stresses at the Inner Face of the Pipe for the Load Case M-4d-D for Horizontal and Vertical Accelerations at 0.96 and 1.28 Sec., Respectively	57
28. Total Stresses at the Outer Face of the Pipe for the Load Case H-d-I for Horizontal and Vertical Accelerations at 0.56 and 0.64 Sec., Respectively	58
29. Total Stresses at the Inner Face of the Pipe for the Load Case H-d-I for Horizontal and Vertical Accelerations at 0.56 and 0.64 Sec., Respectively	59
30. Total Stresses at the Outer Face of the Pipe for the Load Case H-d-D for Horizontal and Vertical Accelerations at 0.64 and 0.56 Sec., Respectively	60
31. Total Stresses at the Inner Face of the Pipe for the Load Case H-d-D for Horizontal and Vertical Accelerations at 0.64 and 0.56 Sec., Respectively	61
32. Total Stresses at the Outer Face of the Pipe for the Load Case H-2d-I for Horizontal and Vertical Accelerations at 0.64 and 0.56 Sec., Respectively	62
33. Total Stresses at the Inner Face of the Pipe for the Load Case H-2d-I for Horizontal and Vertical Accelerations at 0.64 and 0.56 Sec., Respectively	63
34. Total Stresses at the Outer Face of the Pipe for the Load Case H-2d-D for Horizontal and Vertical Accelerations at 0.64 and 1.04 Sec., Respectively	64

List of Figures (Cont'd)

Figure	Page
35. Total Stresses at the Inner Face of the Pipe for the Load Case H-2d-D for Horizontal and Vertical Accelerations at 0.64 and 1.04 Sec., Respectively	65
36. Total Stresses at the Outer Face of the Pipe for the Load Case S-d-I for Horizontal and Vertical Accelerations at 1.76 and 1.04 Sec., Respectively	66
37. Total Stresses at the Inner Face of the Pipe for the Load Case S-d-I for Horizontal and Vertical Accelerations at 1.76 and 1.04 Sec., Respectively	67
38. Total Stresses at the Outer Face of the Pipe for the Load Case S-2d-I for Horizontal and Vertical Accelerations at 1.36 and 1.12 Sec., Respectively	68
39. Total Stresses at the Inner Face of the Pipe for the Load Case S-2d-I for Horizontal and Vertical Accelerations at 1.36 and 1.12 Sec., Respectively	69

INTRODUCTION

Underground pipes and tunnels in urban areas, besides serving as lifelines for the distribution of water, sewage and communication systems, often perform another vital function of providing mass transportation routes. Recent studies have shown that buried water/sewer lifelines have been damaged heavily by earthquakes. For example, in the 1906 San Francisco earthquake, the lack of water due to breakage in the underground pipe lines was mainly responsible for the great fire following the earthquake. Because of the importance of lifelines to the safety and health of the people at the time of disaster, capacity of these structures to survive earthquakes is vitally important. Consequently, lifeline earthquake engineering is drawing considerable attention of the engineering profession (1, 2, 3, 4).

It is becoming increasingly obvious that the behavior of buried lifeline systems is quite different than that of the above ground structures. For example, seismic damage to buildings and dams is mainly due to the horizontal inertial force. In underground piping systems, on the other hand, seismic damage is caused primarily by ground movement and faulting, traveling seismic waves, liquefaction of soil, or difference in stiffnesses of the two horizontally adjacent soil layers (5).

The structural design of most buried water and sewer pipes is based on static analysis. Occasionally passive physical design considerations are used to avoid damage due to seismic effects (6). Since there do not exist any code provisions in the United States for the design of buried pipelines, more research is needed for the development of future design practice and establishment of design guidelines.

As in the case of buried lifelines, little is known about the seismic response and design of tunnel linings. A determination of the earthquake loading on underground linings requires superposition of an induced dynamic loading to the existing static conditions. Methodologies for combining appropriate loading conditions are lacking. One should not design a buried pipe system by the seismic coefficient method, which is sometimes used for the design of above-ground structures, because unrealistically small stresses in the pipe might be obtained due to the neglect of soil-structure interaction.

It has been observed from the field data that a number of parameters related to soil and pipe affect the intensity of damage due to seismic shaking (7). However, the research and experimentation required to thoroughly investigate the influence on pipe stresses of the wide variety of parameters for the vast number of possible combinations of constituent sizes and properties making up the soil-pipe system need a better understanding.

Recently a number of studies have been performed to examine the behavior of buried pipes under seismic loads. An extensive and up-to-date review of the literature is provided in Reference (8). The vast majority of research to date on the seismic stress analysis of buried pipes has used beam theory as a model for the pipe. However, very little attention has been paid to the cross-sectional stress analysis when the seismic wave is traveling perpendicular to the pipe.

As a part of an overall understanding of the behavior of buried pipes under seismic excitation, one particular topic that needs to be investigated is the soil-structure interaction when the seismic wave is traversing perpendicular to the pipe axis. More specifically of concern

are the dynamic stresses caused in the pipe in addition to the static stresses as a result of this interaction. Because these dynamic stresses can be shown to have substantial magnitude, their effects on the buried pipe must be understood before they can be incorporated into the design standard.

Of specific interest to an engineer responsible for the design of a buried pipe or tunnel lining is the magnitude and distribution of stresses in the pipe or tunnel lining. In the case of pipes and tunnels which must be built in urban areas, the problem is further complicated by the fact that these are often shallow and must support the load of the structures at the ground surface in addition to the soil overburden weight, as shown in Figures 1 and 2. One way of avoiding these structural loads is to align the pipes and tunnels below the surface streets but this may not always be possible. Best routes for laying drainage and transportation systems should not necessarily be governed by the arrangement of the surface streets. In downtown metropolitan areas with many highrise buildings, the building foundations usually extend far below the ground surface to bed rock, thus, not contributing much load to the buried structures. On the other hand, in builtup areas of mid- or low-rise structures, pipes and tunnels may be laid below the building foundations and must be designed to support structure foundation loads.

For buried structures that are located in areas of high seismic activity, the maximum design loads may not necessarily be due to static conditions, as described in the previous paragraph, instead they may be caused by the soil-structure-foundation interaction during the occurrence of a severe earthquake. As the safe operation of the underground water and sewage distribution and transportation systems through

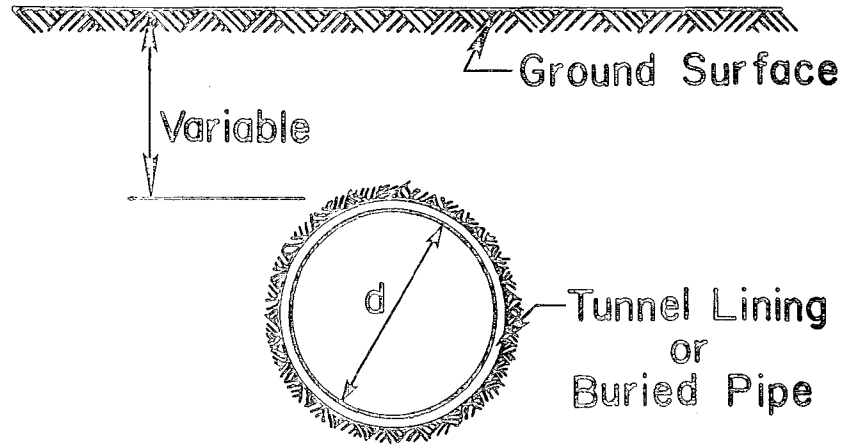


Figure 1. Underground Tunnel or Pipe

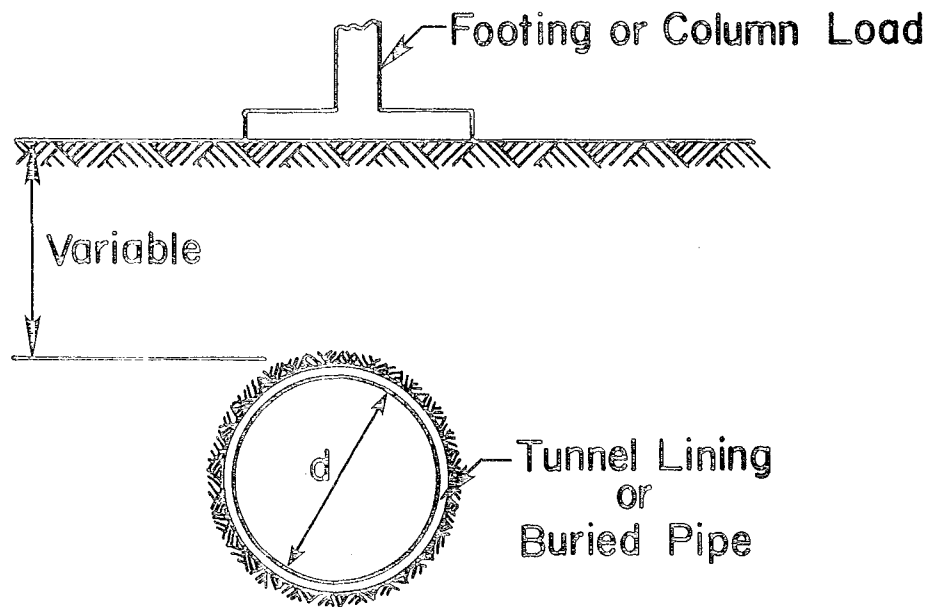


Figure 2. Tunnel Lining or Pipe and Superimposed Surface Load

tunnels in urban areas is vital to the health and safety of the general public before and after an earthquake, it is extremely important that a better understanding of the loads that are transferred to a buried pipe or tunnel lining during an earthquake be developed. In particular, the effects of the concentrated column loads (or the strip line loads) on these structures during an earthquake should be assessed. No studies are available in the literature for the computation of such loads and no recommendations currently exist in the assessment of these loads.

The dynamic interaction of a buried pipe or tunnel lining with the surrounding soil along with the time dependent input of superimposed surface loads from the structure footings due to earthquake acceleration can cause additional loads on the buried structure that may be either extremely critical in design or may not be of substantial magnitude to influence a design. However, no estimates of these loads can be made without actually carrying out some dynamic analyses.

Related Research

In an effort to better understand the dynamic load transfer mechanism for buried pipes or tunnel linings in urban areas when subjected to earthquake forces, some of the related research on the subject is reviewed.

Various attempts have been made during the last 20 years to understand the phenomenon of soil-structure interaction for buried culverts and tunnel linings when subjected to static loads by employing the exact and approximate solution techniques. Linear properties were normally assumed in these analyses both for the buried structure and the surrounding material. Large numbers of experimental and field

investigations have also been undertaken to isolate the effects of various parameters, i.e., the relative stiffness of the soil and structure and the depth of overburden, on pressure distributions around buried pipes. In addition, the finite element method has also been utilized by the engineers and researchers to determine loads around buried pipes and field stresses in the media around cavities. An exhaustive bibliography concerning the estimation of static loads on buried pipes may be found in Reference (9).

Discrete element techniques for elastic-plastic plane problems have been developed recently for metal structures. Elastic-plastic stress-strain relations for soils and rocks have also been proposed in the last few years and have been used to a limited extent in the solution of problems involving consolidation, pressure distribution below foundations and slope stability (10).

Recently, some studies have been made to compute pressure distributions around shallow buried rigid pipes due to static loads considering the soil as an elastic-plastic material (11, 12). A comparison of the results of these analyses with those obtained by an elastic finite element solution indicates that the stresses around shallow buried pipes due to uniformly distributed static surface loads are essentially the same whether the soil is considered elastic or elastic-plastic. The other available published results that describe the state of stress around a buried pipe or tunnel lining using the elastic-plastic finite element analysis are due to Ghaboussi and Rankin (13). These authors also considered only the static load of the soil overburden and the superimposed uniform surface loads, and reached essentially the same conclusion as given in Reference (12) that an introduction of a plastic

behavior for the surrounding soil does not alter the loads on a buried pipe significantly.

Studies regarding the seismic response of oil pipelines that are above the ground level and are supported on friction supports have recently been reported in the literature (14, 15, 16). However, analyses of earthquake effects on above-ground pipelines involve substantially different problems than those which arise in the analyses of underground pipes or tunnel linings. The former support system must allow pipe movement due to thermal as well as pressure forces and at the same time resist the inertial forces that develop during an earthquake. In the later system, on the other hand, the buried pipe or tunnel lining continuously supports and interacts with the surrounding soil during the application of the static and seismic loads.

Also, large numbers of scientific and technical papers have been published in recent years investigating the seismic response of underground lifelines, bibliography of which can be found in References (1) and (8). However, the majority of these studies have analyzed the behavior of underground pipelines using longitudinal models. Of those few which have analyzed transverse models, none has attempted specifically to investigate the effect of frequently encountered superimposed concentrated (or line) surface loads on tunnel linings or buried pipes.

DETERMINATION OF PIPE STRESSES

In order to assess the influence of superimposed surface loads on buried pipes or linings during an earthquake, the effect of the superimposed load in addition to the soil overburden under static conditions should first be determined. This would permit one to estimate the level of dynamic stresses over and above the static stresses under given loading conditions.

As no definite information currently exists in the literature concerning the static loads that act on a buried pipe due to superimposed footing loads, static analysis is initially performed to estimate these loads, as well as the corresponding stresses in the pipe.

Dynamic stresses in the pipe are found with the help of the response of the soil-structure system subjected to an earthquake excitation at the base of the model. This response can either be in terms of the acceleration-time history of the system or the displacement-time history of the structure under investigation. The later type of response is used in this study to determine the equivalent static stresses in the buried pipe. The response of the soil-structure system due to the seismic ground motion is calculated using LUSH (17), one of the available finite element programs.

It has been shown earlier (11, 12, 13) that only linear elastic finite element analyses are necessary in an accurate determination of static loads on buried pipes. Consequently, only elastic analyses are carried out for the determination of static loads in this investigation. However, the effect of non-linear soil properties on pipe stresses in the dynamic analysis is considered.

A basic assumption is made throughout this study that there is a perfect bond between the soil and the buried pipe at the soil-structure interface. The analyses assume that tensile, as well as compressive, normal stresses can be transferred across the soil-structure interface, and that there is no slippage of the soil relative to the pipe at the interface.

Static Analysis

Finite element technique is employed to calculate static stresses in buried pipes due to the soil overburden and superimposed surface loads. As mentioned in the earlier section, only linear elastic material properties have been assumed in the analyses because of the insignificant influence of nonlinear material properties on loads for buried pipes and tunnels.

Loading, Geometry, and Material Properties

It has been shown (12) that the effect of uniformly spaced column loads on a buried pipe can be approximated by an equivalent uniformly distributed line load without introducing an appreciable error. Consequently, only line load is considered in the static analysis. For computation of the footing or column loads acting on the pipe, it is assumed that the pipe is located below a long building directly under the line of columns that are spaced equally apart. The typical line loads at the surface are based on the allowable bearing capacity of various soils (i.e., sandy clay, coarse sand, and dense sand and gravel) and are given in Table 1 (18, 19).

The buried pipe under investigation is assumed to be a circular concrete pipe of 10 feet in diameter and 10 inches in thickness. The

TABLE 1. Load Cases Analyzed for Static and Dynamic Analyses

Load Case	Load		Soil Properties						Strain Independent Soil Properties for Static and Dynamic Analysis	Strain Compatible Soil Properties for Dynamic Analysis Only
	Width	Intensity p	Type	Shear Modulus G (ksf)	Poisson's Ratio ν	Density ρ (pcf)	Fraction of Critical Damping ζ (%)			
1	0	q		500	0.30	120	16	✓*	✓	
2	d	q	Medium (Coarse Sand)	500	0.30	120	16	✓	✓	
3	2d	q		500	0.30	120	16	✓	✓	
4	4d	q		500	0.30	120	16	✓	✓	
5	d	1.6q	Hard (Dense Sand & Gravel)	3500	0.30	125	10	✓	✓	
6	2d	1.6q		3500	0.30	125	10	✓	✓	
7	d	0.533q	Soft (Sandy Clay)	100	0.35	115	16	✓		
8	2d	0.533q		100	0.35	115	16	✓		

d = diameter of the pipe

q = 7.5 kips/ft²

* The check marks (✓) indicate the specific cases that have been analyzed.

depth of burial chosen for the analysis equals one pipe diameter which satisfies the criterion of a shallow buried pipe. For all loading configurations and types of soils considered in the analyses, the concrete pipe is assumed to behave elastically and the buckling phenomenon is not included. The cracking of concrete due to tensile stresses as well as the presence of reinforcement in the pipe are also neglected. The concrete is assumed to have a modulus of elasticity of 3.33×10^3 ksi and Poisson's ratio of 0.2. Eight different load cases, as shown in Table 1, have been analyzed statically to investigate the effects of variable load widths and different soil properties on stresses in shallow buried rigid pipes by elastic analysis. Corresponding to these eight static load cases, dynamic analyses were carried out which will be described in later sections.

Finite Element Model

In order to evaluate static stresses in the pipe due to superimposed surface loads, the finite element technique has been utilized in which it is assumed that a continuous structure can be idealized as an assemblage of a discrete number of finite elements. The finite element technique provides a method for determining the displacements caused by the applied loads on a structure. From these displacements, strains and stresses in the system can be calculated easily (20). It is assumed throughout this study that the structure and loading systems are sufficiently long and a plane strain condition exists.

For the purpose of finding detailed static stresses in the concrete pipe, analysis is carried out in two parts.

In the first part, the whole soil-structure system is modeled for the finite element analysis. In this model, it is assumed that the soil

medium exists up to a depth of one pipe diameter below the pipe. A spacing of twelve pipe diameters between the lateral boundaries has been chosen.** This region with the necessary dimensions and loading is shown in Figure 3. Because of the symmetry of the structure only half of the system is analyzed. The finite element mesh has 205 quadrilateral and/or triangular elements (including 36 elements for the concrete pipe) and 233 nodal points (including 36 boundary nodal points) as shown in Figure 4. Restraints are provided by assigning rollers at the lateral boundaries and hinges at the base. Nodal point displacements along the center line of the pipe circumference caused by the applied surface loads and soil overburden are calculated in the finite element model using an available plane strain finite element computer program.

In the second part of the static analysis, the concrete pipe is modeled for a finite element analysis with a relatively fine mesh as shown in Figure 5. Displacements along the pipe circumference obtained from the first part are imposed as boundary constraints in this finite element model, solution of which leads to stresses and strains in the pipe. With the help of this model it is possible to find the variation of stresses across the pipe thickness as well as the pipe circumference. As the finite element analysis gives stresses at the centroid of each element, a linear extrapolation technique has been utilized to get stresses at the outer and inner faces of the pipe.

** For static analysis, a total lateral dimension of eight pipe diameters for the model would also suffice. However, dynamic analysis criterion restricts the lateral dimension to be equal to at least twelve diameters as discussed in a later section.

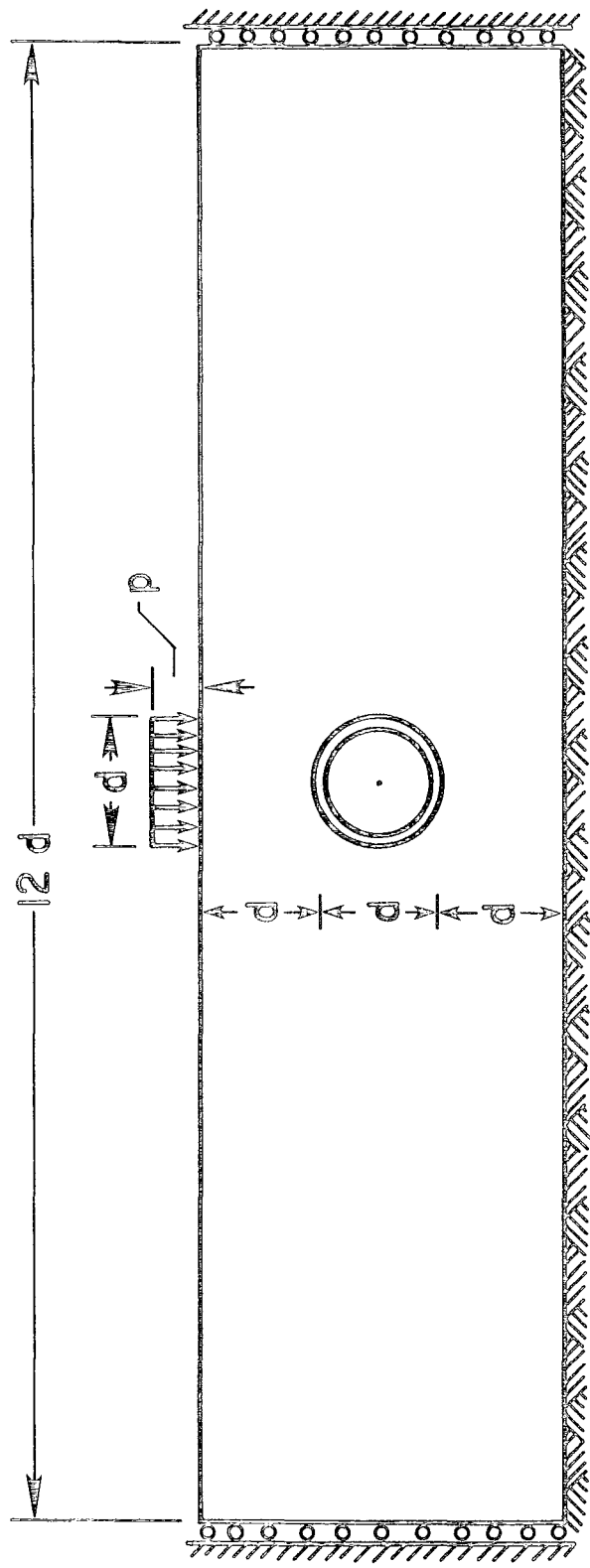


Figure 3. Geometry of the Region Included in the Finite Element Analysis

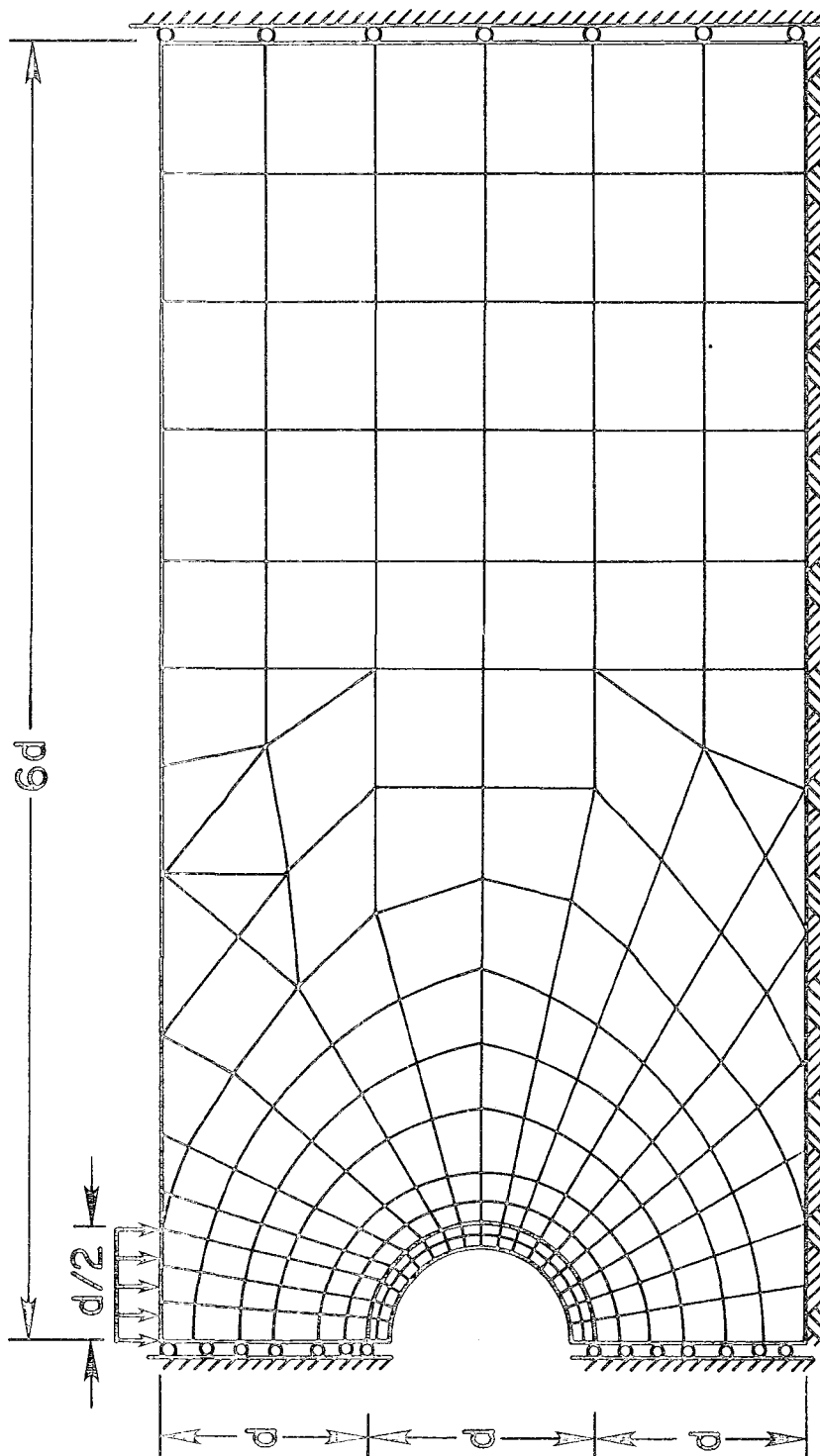


Figure 4. Finite Element Mesh

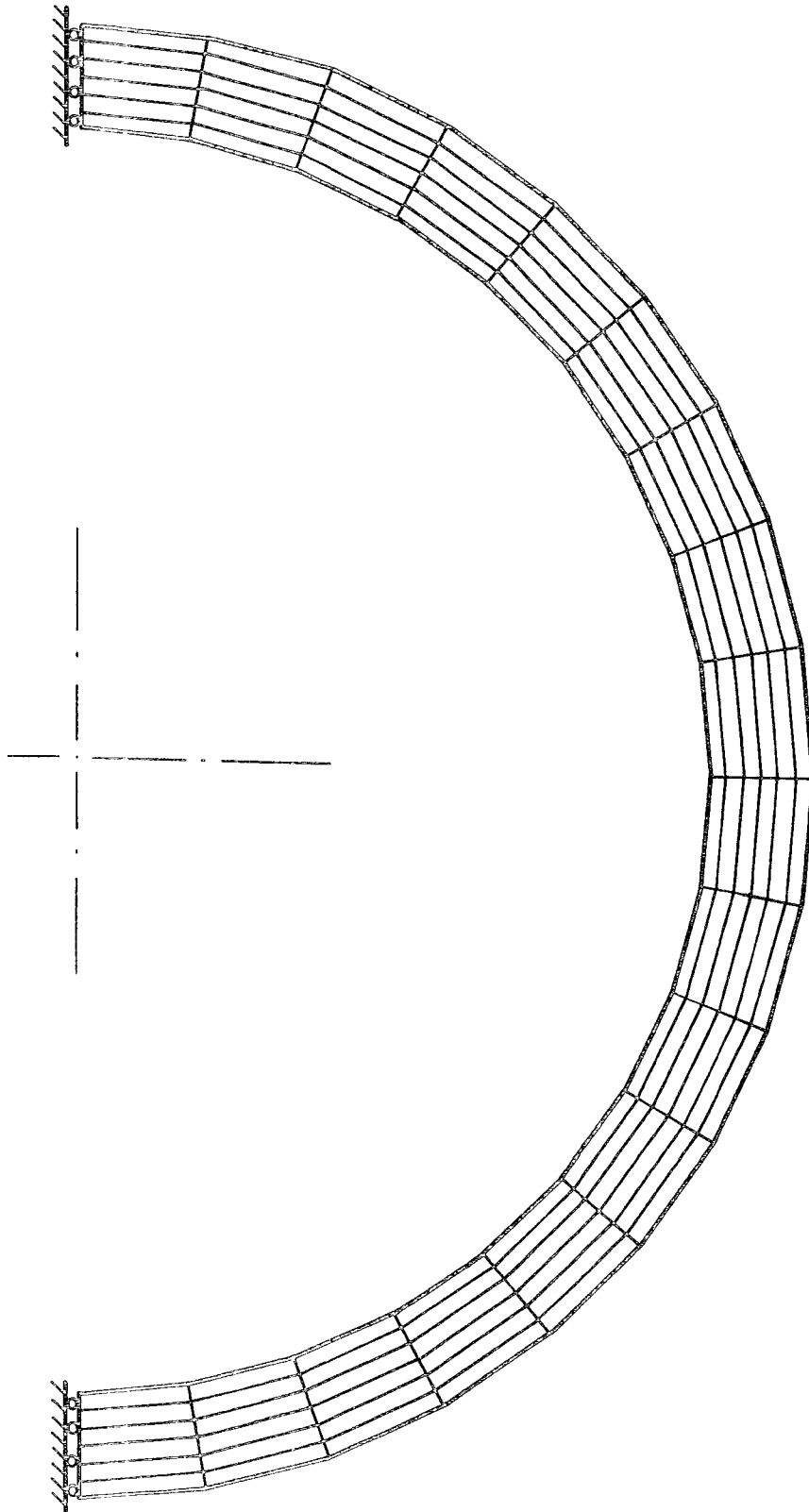


Figure 5. Finite Element Mesh of the Pipe

The above mentioned procedure is followed for each of the cases listed in Table 1.

Dynamic Analysis

An important consideration while finding stresses in the structure under investigation due to seismic effects is the evaluation of the dynamic interaction between the structure and the surrounding soil. This can be accomplished in one of the two ways, either i) by including the effects of the soil on the structural response by representing the soil as a series of springs and dashpots or ii) by modeling the complete soil-structure system as a finite element model. Seed, Lysmer and Hwang (21) have shown that the finite element method offers a better prospect for evaluating the probable behavior of a soil-structure system, and an early availability of a more accurate analysis procedure.

A good finite element analysis should have the capability to incorporate different prescribed damping ratios in every element of the mesh. The mesh should be sufficiently fine to ensure the propagation of all frequencies in the range of interest and extensive enough to provide adequate representation of radiation damping. For the analysis of the soil-structure model under consideration, computations were made by a procedure permitting the use of variable damping in the soil-structure system. This was accomplished by utilizing 'LUSH', a finite element computer program which uses the method of complex response (17).

The solution procedure for the seismic analysis may be summarized as follows: 1) A finite element model for the complete soil-structure system is developed. 2) Response of the finite element model is determined due to an earthquake motion applied at the base of the model.

3) Time histories of the vertical and horizontal displacements at the nodal points along the pipe are plotted. 4) Displacements at a given time that lead to maximum stresses are imposed as boundary constraints on the refined finite element model of the pipe alone to yield the maximum equivalent static stresses in the pipe. 5) Addition of these maximum stresses to those due to the initial static gravity loads then gives total stresses in the pipe under seismic conditions. This procedure is followed for each of the load cases shown in Table 1.

It should be noted here that although in reality there is an interaction between the footing and/or column above the pipe and the pipe-soil system, this interaction is neglected in this study. The objective here is only to ascertain the influence of superimposed surface loads on buried pipes due to the earthquake motion.

LUSH - Theory and Description

LUSH is basically a finite element program designed for earthquake analysis of plane structure. The program, in an approximate manner, takes into account the strong nonlinear effects which occur in soil masses subjected to strong earthquake motions. This is achieved by a combination of the equivalent linear method described by Seed and Idriss (22) and the method of complex response with complex moduli (23). The latter method makes it possible to work with different damping properties in all elements of the finite element model.

The soil-structure model is excited by a specified acceleration-time history at the rigid base. The stiffness and damping of the materials in the model can be chosen to be constant or to vary with the effective shear strain amplitude in each element. The mass distribution

within the model can be either distributed (consistent mass matrix) or concentrated at the nodal points (lumped mass matrix), or it can be any combination of these.

Method of complex response. The equation of motion for undamped vibration of the finite element model can be written as

$$[M] \{\ddot{u}\} + [K]\{u\} = - \{m\} \ddot{y}(t), \quad (1)$$

in which

$\{u\}$ = the nodal point displacements relative to the fixed base,

$\{\ddot{u}\}$ = the corresponding accelerations,

$[K]$ = the stiffness matrix,

$[M]$ = the mass matrix (lumped or consistent),

$\ddot{y}(t)$ = the given input acceleration at the rigid base with the horizontal and vertical components, and

$\{m\}$ = the load vector corresponding to $\ddot{y} = 1$.

Matrices $[M]$ and $[K]$ are symmetric, banded and have the dimensions $NF \times NF$, where $NF = 2 \times$ number of free nodal points.

The method of complex response assumes that the input motion is harmonic with the frequency ω (radians/sec), i.e.,

$$\ddot{y}(t) = \ddot{Y} \cdot e^{i\omega t}, \quad (2)$$

where the amplitude \ddot{Y} may be complex. This implies that for a linear system the response is also harmonic, i.e.,

$$\{u\} = \{U\} \cdot e^{i\omega t}, \quad (3)$$

where $\{U\}$ is a constant, perhaps complex, vector (24). Substitution of Equations (2) and (3) into Equation (1) yields

$$([K] - \omega^2[M])\{U\} = \ddot{Y} \cdot \{m\}, \quad (4)$$

which is nothing but a set of linear equations in the unknowns $\{U\}$.

Equation (4) can be solved by Gaussian elimination if ω is not a natural frequency of the system and the time-dependent response $\{u\}$ follows from Equation (3).

Since the real part of the output corresponds to the real part of the input, the response to

$$\ddot{y}(t) = \text{Re}(\{Y\} \cdot e^{i\omega t}), \quad (5)$$

is

$$u(t) = \text{Re}(\{U\} \cdot e^{i\omega t}). \quad (6)$$

One advantage of the method of complex response is that the viscous damping can be introduced simply by using the complex moduli,

$$\text{shear modulus: } G^* = G(1 - 2\beta^2 + 2i\beta \sqrt{1 - \beta^2}), \quad \text{and} \quad (7)$$

$$\text{Young's modulus: } E^* = E(1 - 2\beta^2 + 2i\beta \sqrt{1 - \beta^2}), \quad (8)$$

in the formation of the stiffness matrix $[K]$. In Equations (7) and (8), β is the ratio of the applied frequency to the natural frequency of the system. Thus, the determinant of Equation (4) cannot vanish and it is possible to find $\{U\}$ for all values of ω . For non-uniform damping, formulas given in Equations (7) and (8) can still be used with different values of G , E and β in each element.

The discrete Fourier transform. Actual earthquake motions are not harmonic. However, if a motion is given as a digitized record with N points at the time interval Δt , it can be decomposed into $N/2 + 1$ harmonics as follows (24):

$$\ddot{y}(t) = \text{Re} \sum_{s=0}^{N/2} \ddot{Y}_s \cdot e^{i\omega_s t}, \quad (9)$$

in which

$$\omega_s = \frac{2\pi s}{N \cdot \Delta t}, \quad \text{for } s = 0, 1, \dots, \frac{N}{2}, \quad (10)$$

and the \ddot{Y}_s are the complex amplitudes

$$\ddot{Y}_s = \left\{ \begin{array}{l} \frac{1}{N} \sum_{k=0}^{N-1} \ddot{y}_k \cdot e^{-i\omega_s k \Delta t}, \quad \text{for } s = 0, s = \frac{N}{2}, \\ \frac{2}{N} \sum_{k=0}^{N-1} \ddot{y}_k \cdot e^{-i\omega_s k \Delta t}, \quad \text{for } 1 \leq s < \frac{N}{2}. \end{array} \right. \quad (11)$$

In this formula

$$\ddot{y}_k = \ddot{y}(k \cdot \Delta t), \quad \text{for } k = 0, 1, \dots, N-1, \quad (12)$$

are the given digitized values of $\ddot{y}(t)$.

The computation of the complex amplitudes, \ddot{Y}_s , in the frequency domain from the given real values, \ddot{y}_k , in the time domain and vice versa is most conveniently done by a superfast algorithm known as the 'Fast Fourier Transform' (25). A limitation on the use of the fast Fourier transform method in LUSH is that N must be a power of 2, (radix 2). Since the motion given by Equation (9) is periodic with period

$$T = N \cdot \Delta t, \quad (13)$$

it is desirable to augment the earthquake by a string of trailing zeros. Moreover, 'quiet zone' at the end of each cycle allows the viscous damping of the system time to attenuate the response from one cycle before the beginning of the next cycle. Since the damping in soils is high, the quiet zone usually needs to be only a few seconds long.

Since superposition is valid for linear viscoelastic systems, the complete solution can be found by simple superposition of each of the

terms of Equation (9) obtained independently by the method of complex response. Suppose $\{U\}_s$ is the solution vector in Equation (4) corresponding to the term $\ddot{Y}_s \cdot \exp(i\omega_s t)$. Then the complete solution

$$\{u(t)\} = \text{Re} \sum_{s=0}^{N/2} \{U\}_s e^{i\omega_s t} \quad (14)$$

can be found by using the inverse fast Fourier transform on the corresponding complex components of $\{U\}_s$. This solves the problem of transient response analysis except for the addition of the rigid base motion to all displacements to form the absolute displacements of all nodal points. This can be done in the time domain or in the frequency domain. LUSH uses the latter method.

Equations (10) and (13) show that the frequencies at which solutions are to be obtained are

$$\nu_s = \frac{s}{T}, \quad \text{for } s = 0, 1, \dots, \frac{N}{2}, \quad (15)$$

where ν_s is the frequency in Hz and T is the total duration of the motion including the trailing zeros of the quiet zone.

The highest frequency is the 'folding' or 'Nyquist' frequency that is given by

$$\nu_{N/2} = \frac{1}{2\Delta t}, \quad (16)$$

and is the highest frequency which can be represented by data digitized in the time interval Δt .

According to the above method, Equation (4) would have to be solved for $\frac{N}{2} + 1$ frequencies. However, this number can be reduced by cutting off the higher frequencies. Equation (16) shows that for earthquake records digitized at very small time intervals, 'Nyquist' frequency is very high. Such high frequencies are usually not of interest and can

be neglected by setting the high frequency terms in Equation (14) equal to zero, or redigitizing the earthquake record with larger time intervals, thus avoiding the solution of Equation (4) for these frequencies. The redigitizing of an earthquake record for larger time intervals, if necessary, can be done by the computer program SHAKE (26).

The number of frequencies at which the solution need to be found can be reduced further by interpolation in the frequency domain. Suppose, instead of Equation (4), one solves

$$([K] - \omega^2[M])\{A\} = -\{m\} , \quad (17)$$

over the range of frequencies. Then, the components of $\{A\}$, here called amplification functions, will be smooth functions of ω . One can, therefore, proceed by evaluating $\{A\}_s$ at say every 4th frequency ω_s for $s = 0, 4, 8, \dots$, and then obtain the intermediate amplification functions by interpolation. Experience has shown that linear interpolation on the inverse of the amplification functions gives good interpolated values even near the natural frequencies as long as there is good separation between the latter. Typically, it has been found necessary to solve Equation (17) for every 4th or 8th frequency.

The equivalent linear method. The above solution procedure makes extensive use of superposition and is, therefore, applicable only to linear visco-elastic systems. However, the large shear deformations which occur in soils during strong earthquakes introduce significant nonlinear effects. This has been taken care of by introduction of the equivalent linear method by Seed and Idriss (22). In this method an approximate nonlinear solution is obtained by a linear analysis wherein stiffness and damping used in the analysis are so chosen so as to be

compatible with the effective shear strain amplitudes at all points of the system. Seed and Idriss (27) have published data on strain-compatible soil properties for typical clays and sands. This data has been summarized in Table 2 and is graphically shown in Figures 6 and 7. These strain dependent properties are incorporated within Subroutine CURVE52 of LUSH in the form of DATA statements.

The equivalent linear method uses the above data as follows: A set of shear moduli and damping values is estimated for each soil element of the finite element model. The system is analyzed using these properties and the shear strain history is computed in each element of the model. From these time histories the effective shear strain amplitudes are estimated (in LUSH by assuming that γ (effective) = factor * $|\gamma|$ (maximum)) in each element and Table 2 is consulted to see if the strain level is compatible with the values of shear moduli and damping used in the response evaluation. If the soil properties are not compatible the table is entered to provide improved values of shear moduli and damping for the next iteration and the process is repeated until convergence is reached, usually within 3 to 5 iterations. The response from the last iteration is taken as being the nonlinear response.

If the material properties are assumed to be strain-independent, then Subroutine CURVE52 in the program is bypassed and there is no need for an iterative procedure.

Program description. The computer program LUSH was developed by Lysmer, Udaka, Seed and Hwang of the Department of Civil Engineering, University of California at Berkeley. The program used for the purpose of analysis in this study is LUSH2 version and is written in FORTRAN IV language.

Table 2. Strain-Compatible Soil Properties

Effective Shear Strain $\gamma_{eff}(\%)$	Log (γ_{eff})	Shear Modulus Reduction Factor*		Fraction of Critical Damping (%)	
		Clay	Sand	Clay	Sand
$\leq 1. \times 10^{-4}$	-4.0	1.000	1.000	2.50	0.50
3.16×10^{-4}	-3.5	0.913	0.984	2.50	0.80
1.00×10^{-3}	-3.0	0.761	0.934	2.50	1.70
3.16×10^{-3}	-2.5	0.565	0.826	3.50	3.20
1.00×10^{-2}	-2.0	0.400	0.656	4.75	5.60
3.16×10^{-2}	-1.5	0.261	0.443	6.50	10.0
1.00×10^{-1}	-1.0	0.152	0.246	9.25	15.5
0.316	-0.5	0.076	0.115	13.8	21.0
1.00	0.0	0.037	0.049	20.0	24.6
3.16	0.5	0.013	0.049	26.0	24.6
≥ 10.00	1.0	0.004	0.049	29.0	24.6

* This is the factor which has to be applied to the shear modulus at low shear strain amplitudes (here defined as 10⁻⁴ percent) to obtain the modulus at higher strain levels.

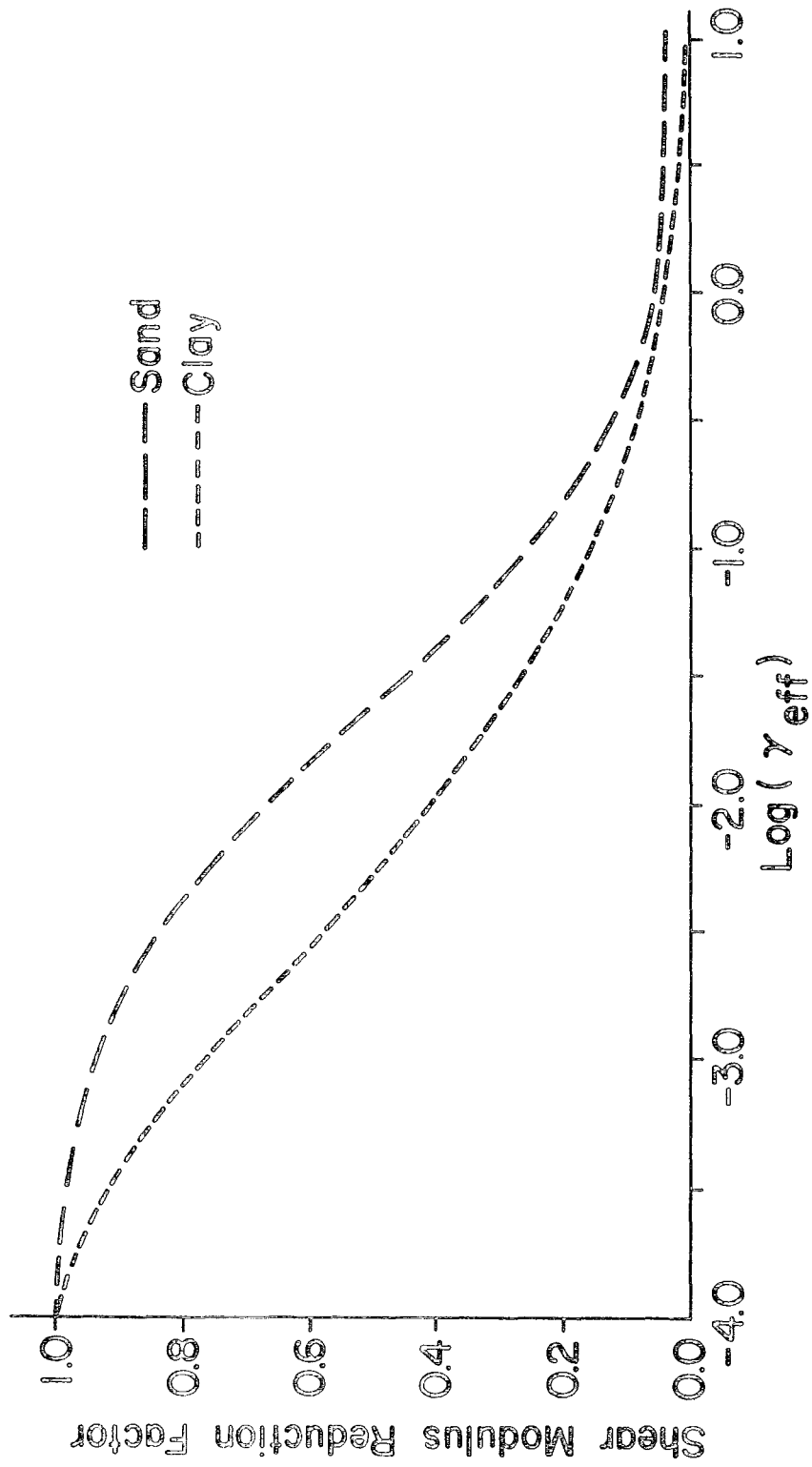


Figure 6. Strain-Compatible Shear Modulus Reduction Factor

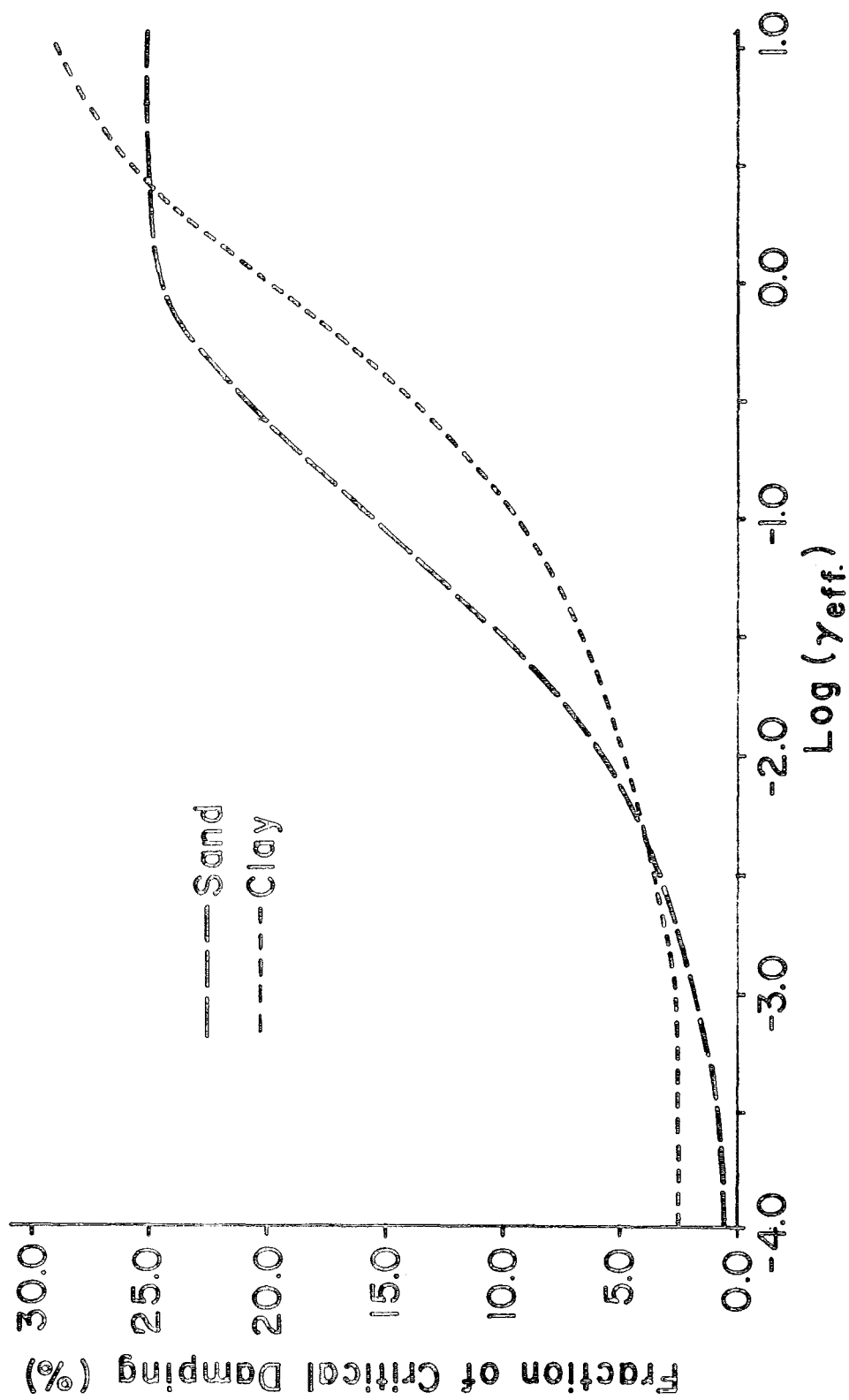


Figure 7. Strain-Compatible Critical Damping Ratio

The program operates in three modes, i.e., Mode 1, Mode 2, and Mode 3. Mode 1 initializes the program and stores the input data, forms mass and stiffness matrices, computes all amplification functions from Equation (17), and estimates new soil properties from Subroutine CURVE52 if these are strain dependent. Specified number of iterations are carried out in this mode to obtain strain-compatible material properties. At the end of Mode 1, all the information is stored permanently in TAPE 1 for subsequent use. Since the record in TAPE 1 is complete and permanent, this tape can be stored indefinitely for retrieval of the motion-time history of any nodal point.

In Mode 2, the contents of TAPE 1 are copied onto TAPE 2. The information in TAPE 1 can then be recovered to generate additional output for any new input motion without repeating the costly finite element procedure used in Mode 1. Also, additional iterations on soil properties at higher frequencies can be initiated. The resulting amplification functions are written on TAPE 1.

Mode 3 is used to obtain the combined response of different horizontal and vertical input motions as follows: First the horizontal response is determined using Mode 1 and/or Mode 2. This produces a TAPE 1 containing the horizontal response. This tape is then read in Mode 3 which transfers the horizontal response to TAPE 2, reads the vertical input motion, and produces the vertical response on TAPE 1. The two physical tapes TAPE 1 and TAPE 2 may then be read by a separate auxiliary computer program COMBINE, which superimposes the two motions.

Both LUSH, operating in any mode, and COMBINE can output the nodal point motions, as punched or printer-plotted displacement-or acceleration-time histories or as velocity and acceleration response spectra.

Development of the Finite Element Model for Dynamic Analysis

Criteria for selecting various input data are discussed in this section as the response of the system may be rather sensitive to some of the parameters.

Selection of model dimensions and boundary conditions. As mentioned earlier, LUSH is a finite element program designed for earthquake analysis of plane structures. Since the soil-pipe system under investigation can be represented as a planer structure, the finite element model for the dynamic analysis is essentially similar to that used in the static analysis. However, some considerations involved in the development of the finite element mesh for the dynamic analysis, which differ from those in the static case, are discussed here.

The overall dimensions of the finite element mesh influence the response of the structure due to reflections from the boundaries. Hence, it is necessary to use a finite element model which extends a sufficient distance away from the structure to ensure that radiation damping effects are properly accounted for. If the boundaries of the mesh are placed too close to the structure, some of the energy which should dissipate from the system will be reflected back, thereby changing the response.

The rigid base, where a sudden increase in stiffness with respect to the depth occurs, should be located at a soil depth below the structure at least equal to the width of the structure. Side boundaries should be defined at a distance far enough away to achieve a free field condition. It is usually sufficient to place the lateral boundaries at a distance of 2.0 to 2.5 times the depth of the model away from the structure. This rule applies only to cases with considerable

damping and assumes that the boundary conditions have been chosen as discussed below.

In order to simulate the existence of horizontal soil layers outside the vertical boundaries, it is necessary to impose special boundary conditions on these boundaries. If the input motion is horizontal, the motion in the free field will correspond to vertically propagating shear waves and all motions in the free field will be horizontal. This condition can be simulated by imposing the boundary conditions that all nodal points on the vertical boundaries can move in the horizontal direction only. Similarly, if the input motion is vertical, the boundary conditions imposed allow movement in vertical direction only at the lateral boundaries.

The above boundary conditions can be used to take advantage of the symmetry in the finite element model. Suppose the symmetric model shown in Figure 8(a) is to be analyzed for the combined action of the horizontal input motion $\ddot{h}(t)$ and the vertical input motion $\ddot{v}(t)$. It is then sufficient to analyze one half of the structure with the boundary conditions shown in Figures 8(b) and 8(c). The horizontal response is found first, using Mode 1 or Mode 2 and the model shown in Figure 8(b). Then the vertical response is found, using Mode 3 and the model shown in Figure 8(c), and the two solutions can be added by the computer program COMBINE.

Another aspect of the finite element analysis requiring careful control is the choice of the element size in the finite element mesh, especially in the vertical direction. Kuhlemeyer and Lysmer (28) found that the dimensions of the elements in the direction of wave propagation have a major influence on the frequencies of motions that can be

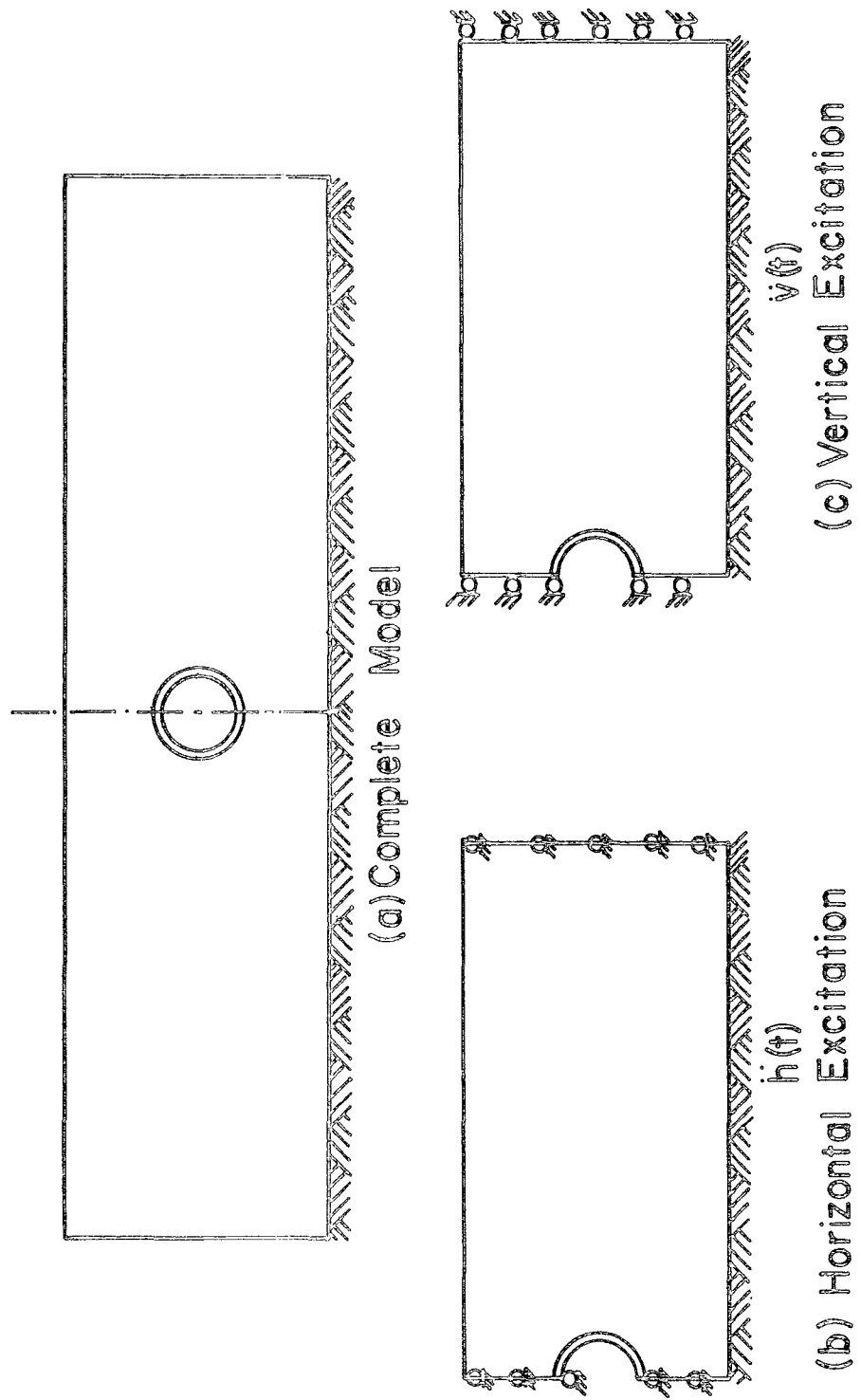


Figure 8. Boundary Conditions Used for Horizontal and Vertical Excitations

transmitted, with larger elements being unable to transmit motions with high frequencies and correspondingly short wavelengths. In fact, they proposed the empirical rule that the required mesh size for effective transmission of any motion should not be more than one-quarter, or preferably one-eighth, of the wave-length of the motion. Experience with LUSH has shown that a good rule is to choose the element size in the vertical direction which is less than

$$h_{\max} = \frac{1}{5} \lambda_s = \frac{1}{5} \frac{v_s}{v_{\max}}, \quad (18)$$

where λ_s is the wave length of the shortest shear wave, v_s is the shear wave velocity in the element, and v_{\max} is the highest frequency considered in the analysis. The computed response is less sensitive to the choice of the element size in the horizontal direction which can be chosen several times larger than the dimension given by Equation (18).

Input motion. The input motion at the base of the finite element model in a typical problem is provided as a digitized earthquake acceleration record with specified maximum acceleration and duration. Majority of the earthquake motions are recorded at the ground surface or at some elevation in the superstructure depending upon the location of the accelerometers at the site. To get the acceleration record at the base of the soil profile for use as input in the analysis, deconvolution analysis is generally performed. However, the earthquake record used in this study is an acceleration-time history of a hypothetical earthquake that is given in the LUSH manual and, therefore, does not require any deconvolution analysis.

As mentioned in an earlier section, the input motion must be augmented by trailing zeros and the total number of points at which the

acceleration is defined must be a power of two. The number of trailing zeros in a record is considered sufficient if the output motions computed by LUSH are attenuated within the selected period of the input motion. The earthquake record for the purpose of this study has 64 points digitized at time intervals $\Delta t = 0.04$ sec. By introducing 64 trailing zeros at the end of the earthquake record to provide the desirable quiet zone, the number of discrete points have been increased to $2^7 = 128$. The ordinates of the earthquake record have been scaled to provide a maximum acceleration of 0.15g as shown in Figure 9. The Nyquist frequency for this earthquake record with $\Delta t = 0.04$ sec. can be computed from Equation (16) and equals 12.5 Hz.

Maximum frequency. The highest frequency to be considered in the analysis is the most important of all decisions since the frequency will more than anything else affect the accuracy of the response, the finite element dimensions to be selected in the analysis and the cost of the analysis. Typical values for the highest frequency are 8 Hz for earth dams and 25 Hz for stiffer systems like nuclear power plants. Using the results of a preliminary investigation, a maximum frequency of 12 Hz is selected for the soil-pipe system under consideration.

Interpolation control. The actual number of points at which intermediate amplification functions given by Equation (17) can be obtained by interpolation without introducing significant error should be determined by a trial and error procedure.

An example problem consisting of two columns of five rectangular elements and 11 nodes was considered for the purpose of finding the effect of the number of intermediate points (at which the amplification functions are obtained by interpolation) on the response of this

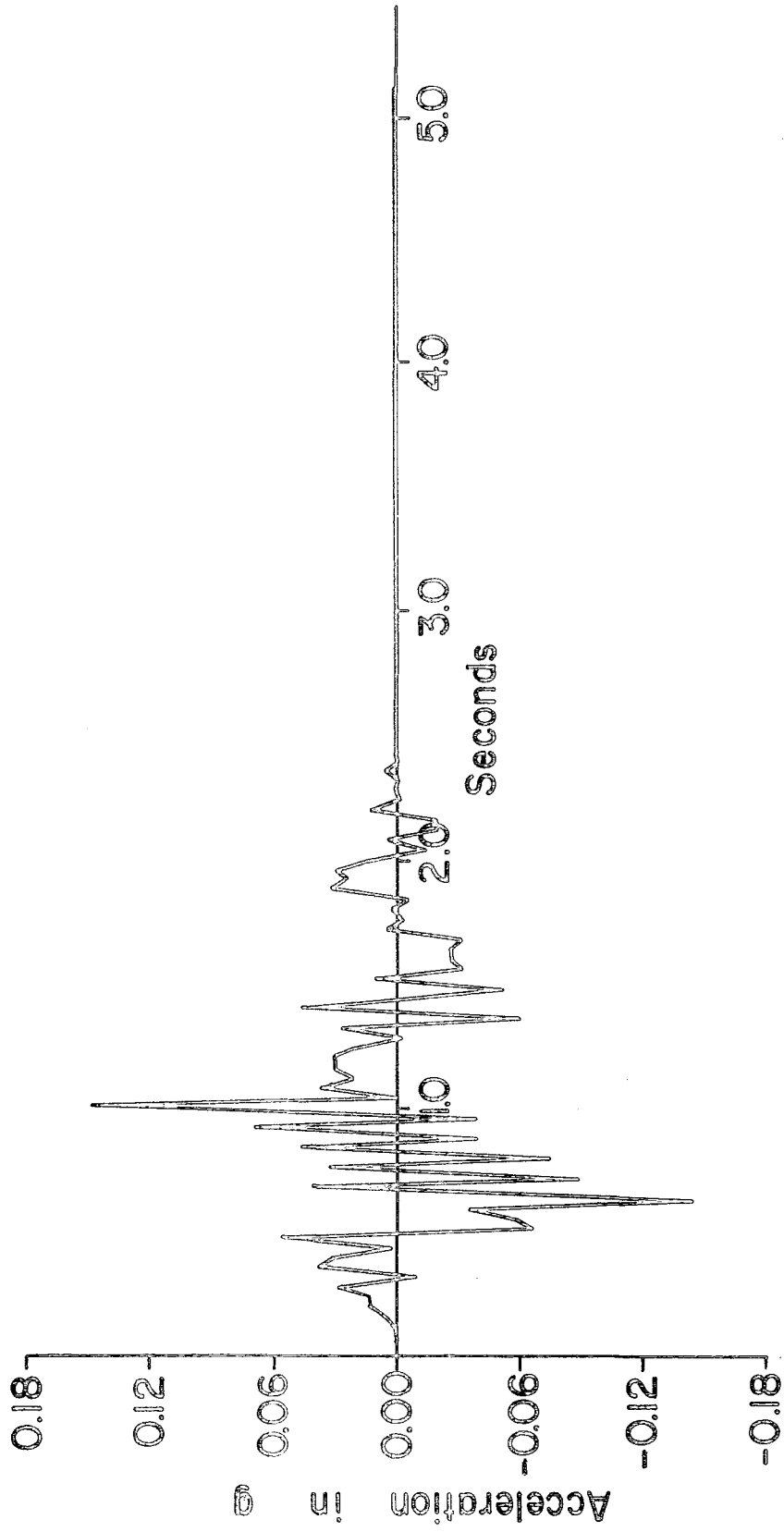


Figure 9. Earthquake Acceleration Time History

system using a maximum frequency of 12 Hz. It was observed that the percentage difference in the response acceleration at a particular node was 7% when the number of the intermediate points was increased from 2 to 4. However, this difference increased to approximately 30% with an increase in the number of the intermediate points from 4 to 8. Therefore, for the purpose of the analysis in this study, Equation (17) was solved at every 4th frequency point to obtain an acceptable solution with minimum amount of computational effort.

Mass matrix. There have been some findings in the literature which state that the use of consistent mass matrix provides a better accuracy than the lumped mass matrix (28). However, Clough (29) states, "experience shows that the lumped mass formulation must be used to obtain reliable results in any wave propagation problem". The two experiences are contradictory and further accuracy studies that separate the effects of the various approximations are required in order to further clarify the disagreements. As the major benefit in using the lumped mass matrix to solve transient problems is a saving in the computer storage space, this method would be used in the finite element analyses carried out in this research.

Material properties. The basic material properties to be specified for each finite element are the unit weight, Poisson's ratio, the fraction of critical damping, and the shear modulus at small strains, here defined as $\gamma = 10^{-4} \%$. The appropriate value for each of these quantities were found from the related texts (18, 19), and are listed in Table 1. If the soil properties are considered strain dependent, then estimates must also be made for the shear modulus to be used during the first iteration. It is possible to obtain these estimates using the

column studies on soil. As no column studies were performed, the values of the shear modulus used for each element during the first iteration in the analysis was chosen as 40-50% of the maximum.

For strain independent materials, the values for the shear modulus and fraction of critical damping remain constant.

Iterations on soil properties. From experience it has been shown that convergence to within 5-10% on the shear moduli and damping values can be expected within 2 to 3 iterations. Savings in the computational effort can be achieved by solving Equation (17) for amplification functions at fewer frequency points during initial iteration(s) in Mode 1. This can be done by choosing a frequency lower than the desired highest frequency, and by solving for the amplification functions at larger intervals. Solutions in Mode 1 have been obtained for 10 Hz at every 8th frequency point for the analyses presented in this study. In Mode 2 and 3, on the other hand, a maximum frequency of 12 Hz has been utilized to solve the amplification functions for every 4th frequency.

Solution Procedure

Procedure similar to that used in the static analysis has been utilized for finding equivalent static stresses due to seismic loading. As discussed earlier in this chapter, the soil-structure system is represented by a plane strain finite element model with surface loads at the top as shown in Figure 4. This model is analyzed for 14 different load cases, where in eight cases strain-independent soil properties have been used (Table 1), and in the remaining cases the soil is assumed to have strain-compatible material properties. Displacement-time histories along the pipe circumference are found due to the hypothetical earthquake motion, shown in Figure 9, applied as a base acceleration

in the horizontal and vertical directions using the LUSH program for all load cases shown in Table 1. Base earthquake acceleration in the vertical direction is assumed to be 66.6% of the horizontal acceleration in these analyses. Typical plots for displacement-time history due to horizontal and vertical excitation are shown in Figures 10 and 11.

As in the static case, the concrete pipe alone is modeled for a quasi-static finite element analysis with the fine mesh as shown in Figure 5. Nodal point displacements along the pipe circumference, obtained at a given time from the displacement-time histories, are imposed as boundary constraints on the finite element model of the pipe which is solved to yield the element stresses. This procedure is repeated at several relevant time instances, e.g., 0.56, 0.64 and 1.04 seconds, to obtain maximum stresses in the pipe for horizontal and vertical accelerations separately, for each load case.

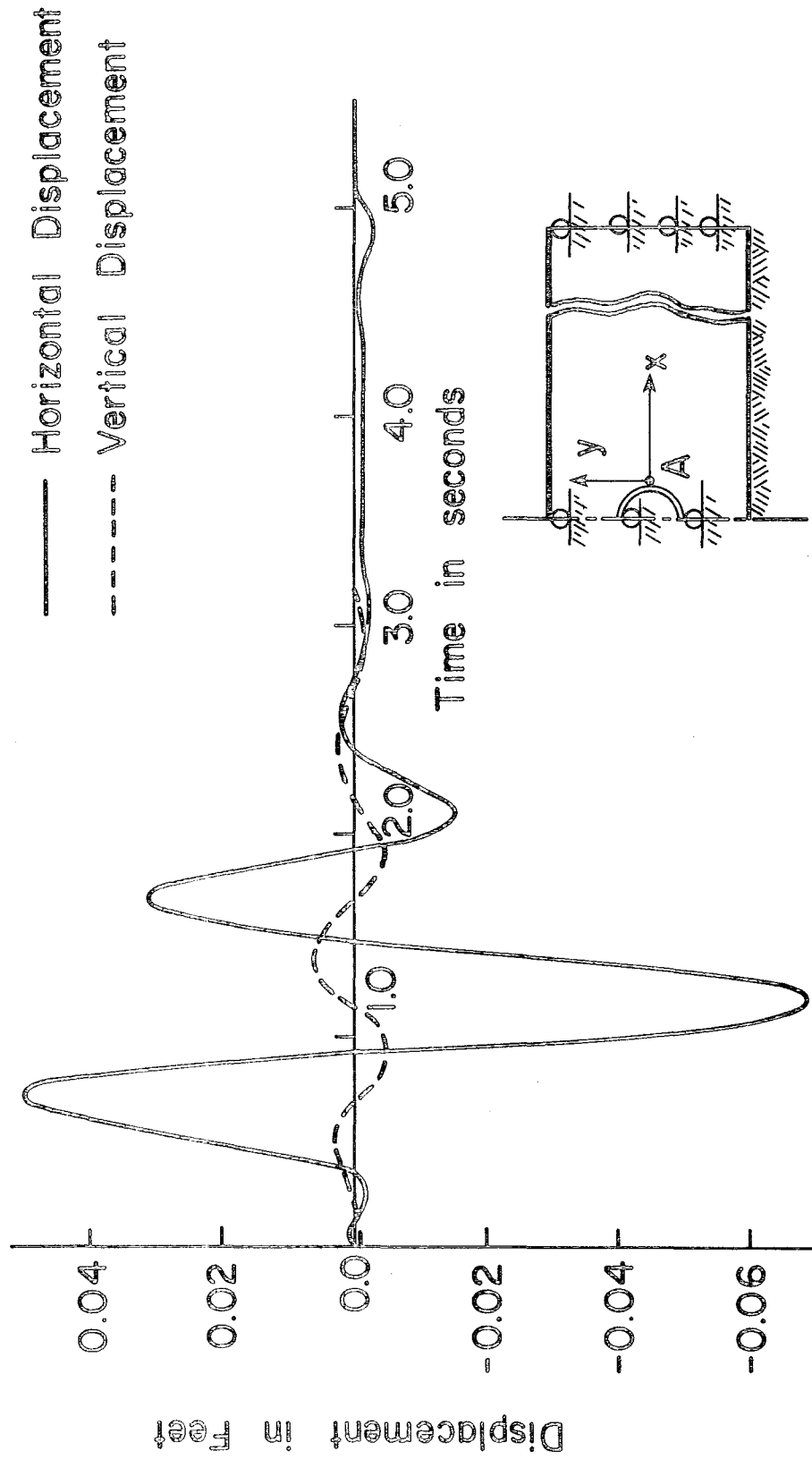


Figure 10. Typical Displacement Time History at Point A Due to Horizontal Excitation

— Horizontal Displacement

- - - Vertical Displacement

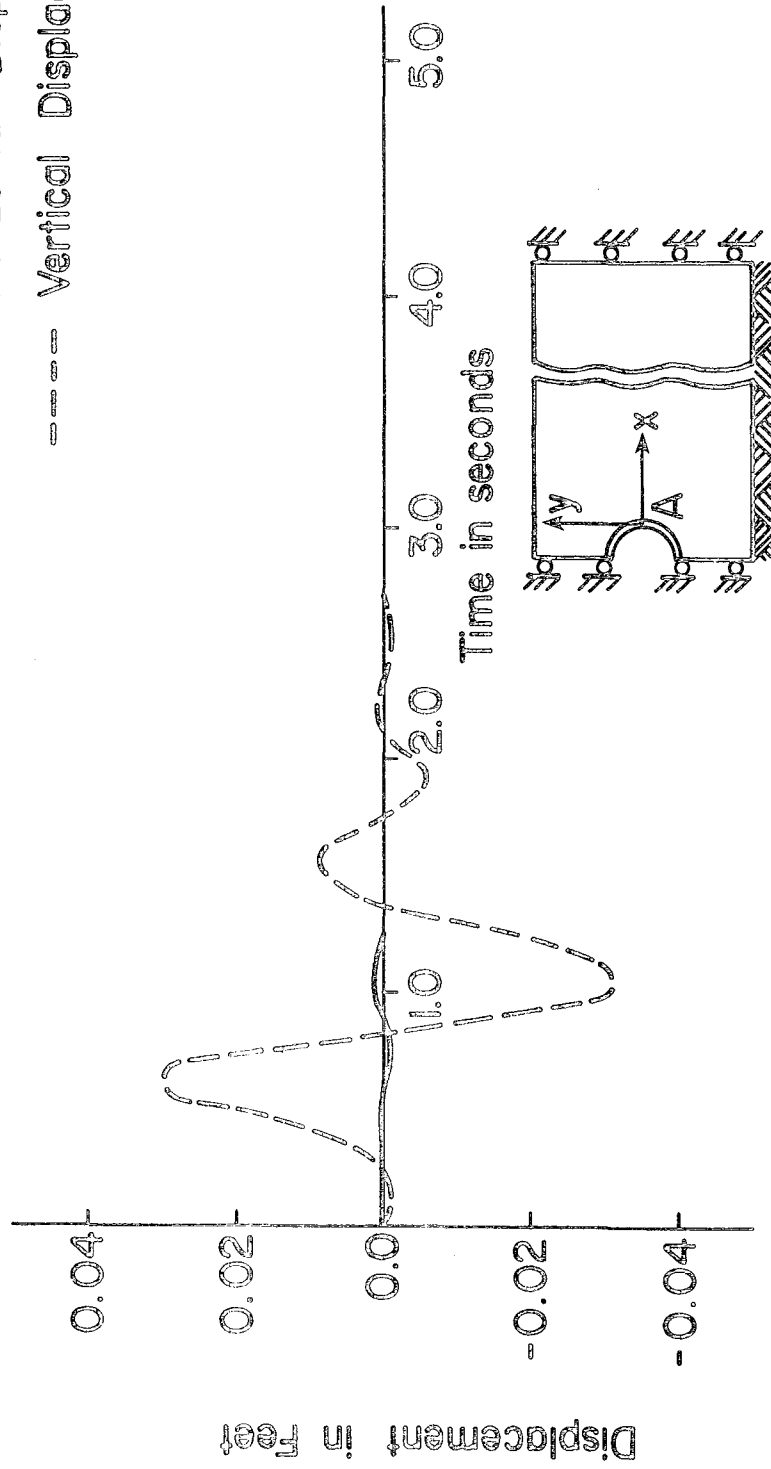


Figure 11. Typical Displacement Time History at Point A Due to Vertical Excitation

EVALUATION OF PIPE STRESSES

General Considerations

Any soil-structure system, when subjected to a random input motion as an earthquake, yields a random response. The resulting stresses at a given point in the system are random in nature due to this response and, therefore, fluctuate between compression and tension.

The input motion in this study, given by the earthquake accelerogram, is applied along the horizontal and vertical directions to yield two independent random responses. In most cases, the maximum stresses as a result of these two input motions do not occur at the same time. However, it is still possible for the maximum stresses due to both acceleration components to occur at a particular time instance because of the random phase difference between the acceleration components in the horizontal and vertical directions in majority of the earthquakes. Hence, the maximum quasi-static stresses due to the horizontal and vertical accelerations, even if these occur at different times, are added to the existing state of stress from static loads to yield the worst possible combination of stresses.

The influence on the normal tangential stresses in the pipe due to a variation in the width of the superimposed surface load for three different types of soils using strain-compatible and strain-independent material properties has been investigated in this study. Fourteen different cases, as shown in Table 1, have been analyzed. Three different types of soils considered in the analyses are i) dense sand and gravel (hard), ii) coarse sand (medium), and iii) sandy clay (soft).

Since the soil properties encountered most commonly in the field at shallow depths are similar to those assumed for the medium soil in this study, cases with these properties are analyzed extensively. For this soil, superimposed surface loads over widths of d , $2d$ and $4d$ are applied with a uniform intensity of $q = 7.5 \text{ kips/ft}^2$, and the pipe response is determined using strain-compatible as well as strain-independent soil properties. In addition, one case without any superimposed load is also investigated.

For soils other than coarse sand, the intensity of superimposed surface loads acting on the pipe is assumed to be larger than q for hard soils and smaller than q for soft soils due to larger and smaller bearing capacities of these soils, respectively. Surface loads of 12 kips/ft and 4 kips/ft, respectively, are assumed in the analyses for dense sand and gravel (hard), and sandy clay (soft). For each soil, load widths of d and $2d$ are considered. As unrealistically small values of shear modulus are obtained after few iterations with the use of strain-compatible material properties for soft soils, only strain-independent material properties are considered in this case.

Nomenclature and Sign Convention

Each load case is designated separately to facilitate identification, where the following procedure is utilized for the purpose of nomenclature. Each of the soils is designated by a letter, e.g., H for hard, M for medium, and S for soft. Similarly, letters I and D are used to denote strain-independent and strain-compatible soil properties, respectively. The magnitude of the column or footing load acting at the ground surface, in each case, is denoted in terms of the width of a uniformly distributed load, e.g., $2d$ for a uniformly distributed

load of width $2d$ and 0 for no superimposed load. Thus, a case of uniformly distributed superimposed load of width $2d$ for hard soil using strain-compatible material properties may be designated as H-2d-D.

Stresses found after analyzing all the load cases are plotted and tabulated to facilitate the evaluation of the pipe behavior under different loading conditions. Since the surface load intensity used for different soils is different, non-dimensional stresses are presented for the purpose of comparison. Tangential stresses obtained in each load case are non-dimensionalized with respect to the corresponding load intensity, p , and are given by

$$\bar{\sigma}_{\theta} = \frac{\sigma_{\theta}}{p} \quad (19)$$

Non-dimensional tangential stresses at the outer and inner faces of the pipe are plotted separately for each loading case, in which tension and compression are assigned positive and negative signs, respectively.

Maximum Stresses and Dynamic Load Factors

Since the input motion is random, as discussed earlier in this chapter, equivalent static stresses at a given point on the pipe due to horizontal and vertical excitations may accentuate or relieve the existing state of stress due to static loads. This leads to various combinations of stress configurations in the pipe for each loading case; for example, stresses due to static plus/minus horizontal plus/minus vertical seismic loads. Since it is impractical to show all these combinations on each plot, only pertinent combinations which lead to maximum compression and/or tension are shown in Figures 12 to 39. Letters C and T in these graphs, respectively, denote maximum compression and maximum tension around the pipe circumference. Stresses at inside and

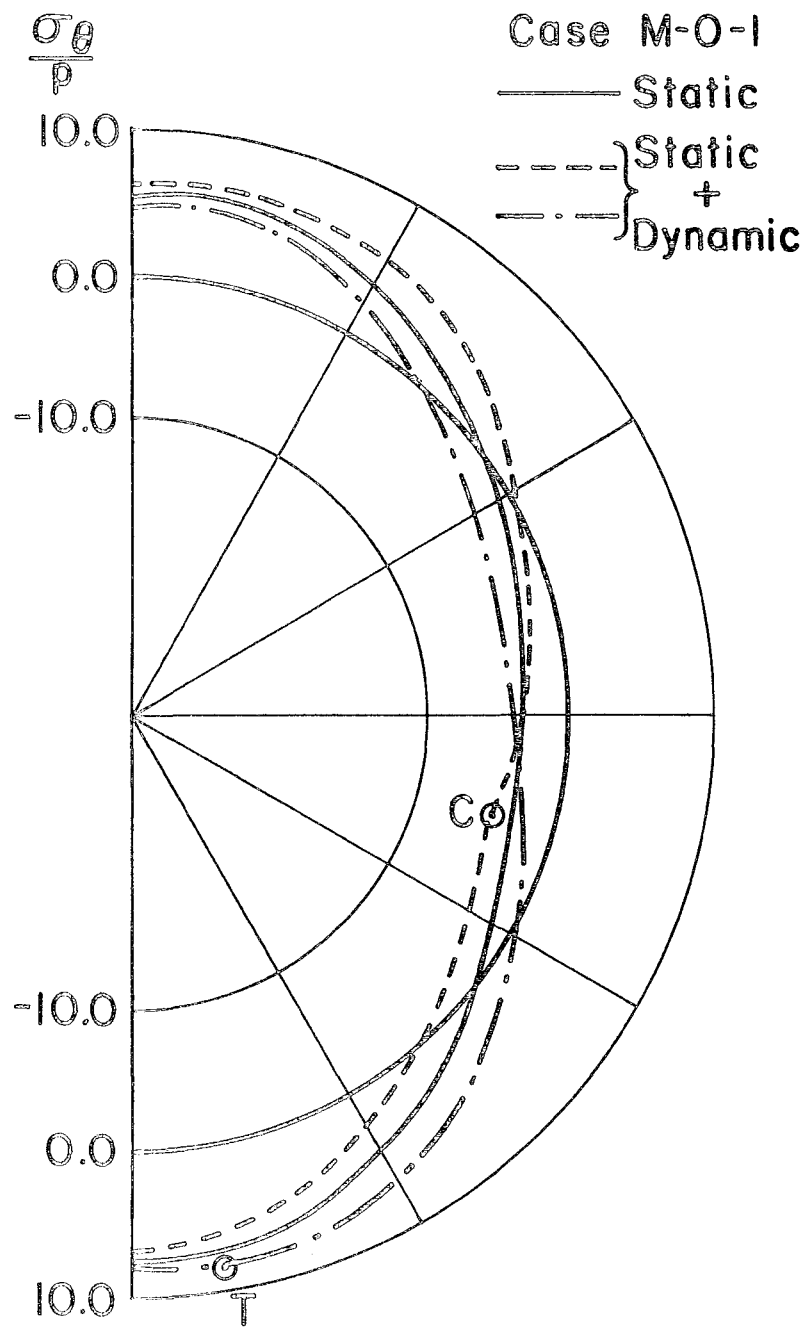


Figure 12. Total Stresses at the Outer Face of the Pipe for the Load Case M-0-1 for Horizontal and Vertical Accelerations at 0.64 Sec.

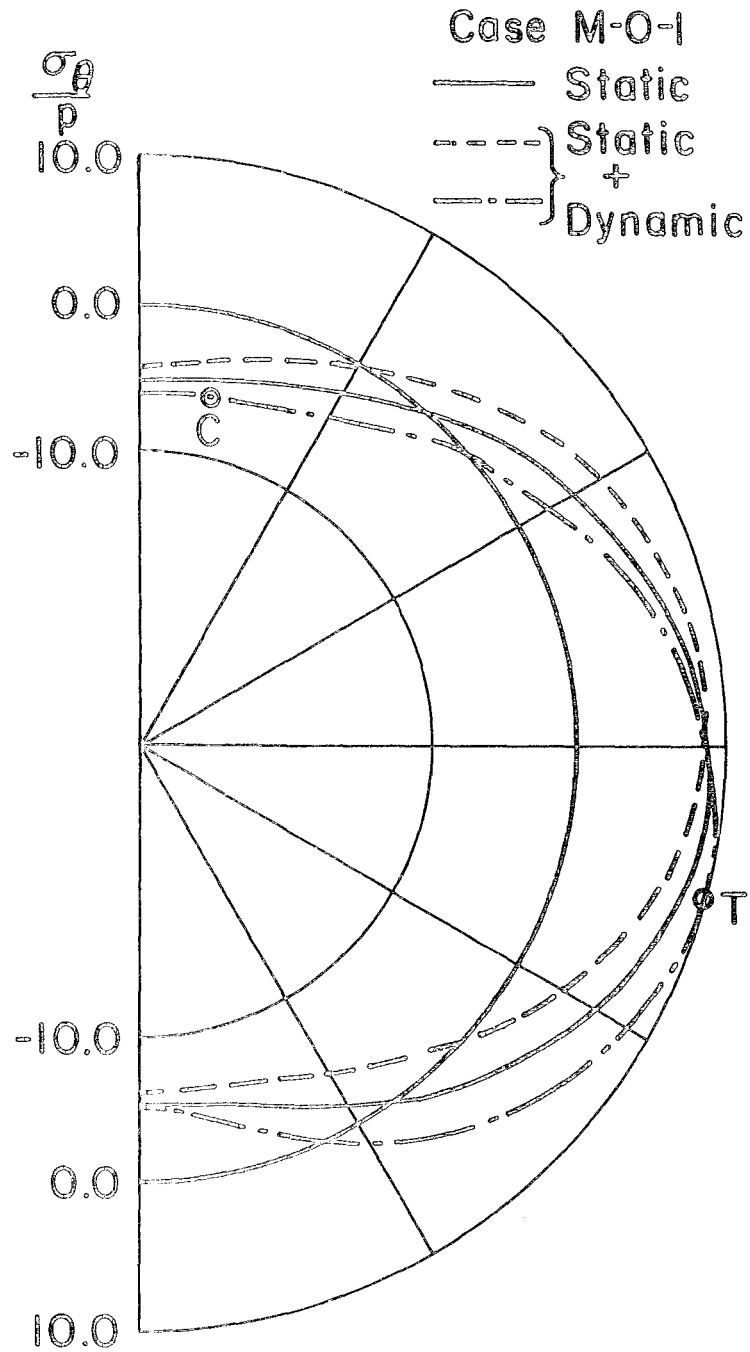


Figure 13. Total Stresses at the Inner Face of the Pipe for the Load Case M-0-1 for Horizontal and Vertical Accelerations at 0.64 Sec.

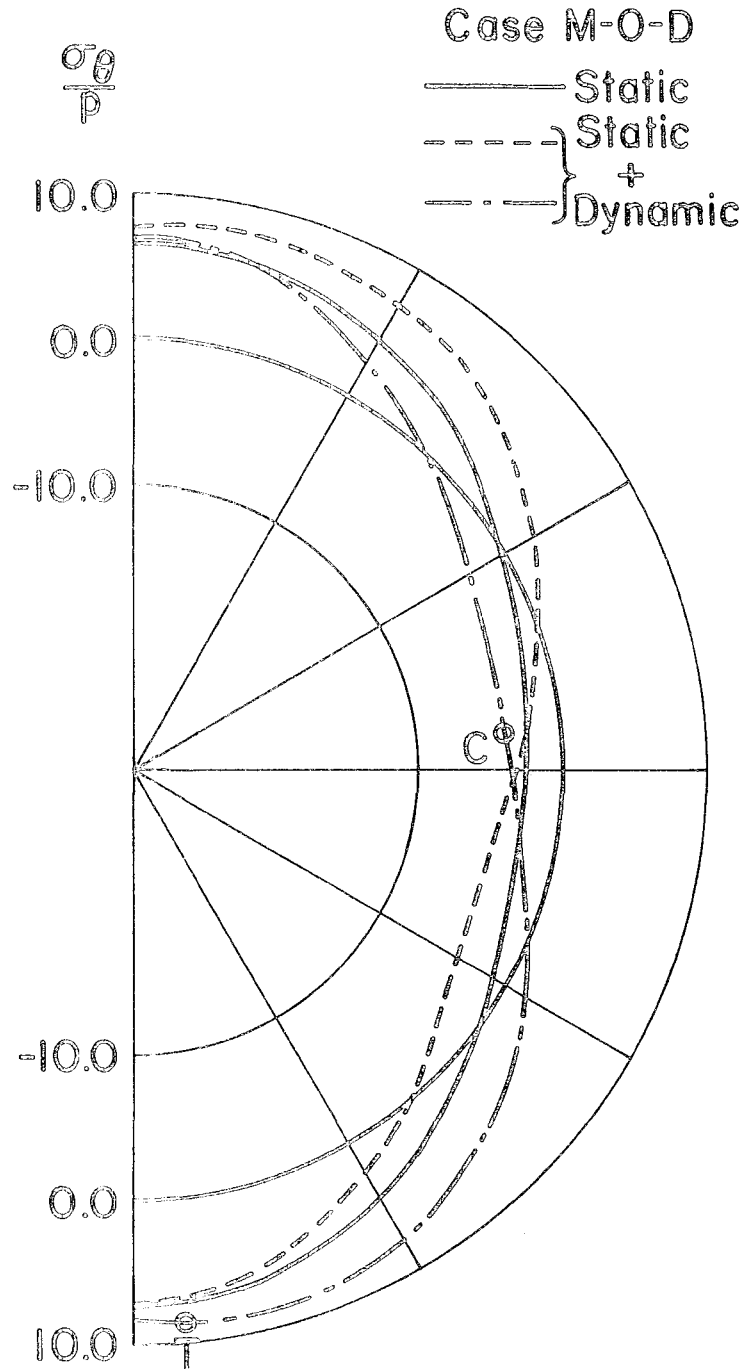


Figure 14. Total Stresses at the Outer Face of the Pipe for the Load Case M-O-D for Horizontal and Vertical Accelerations at 1.12 and 0.64 Sec., Respectively

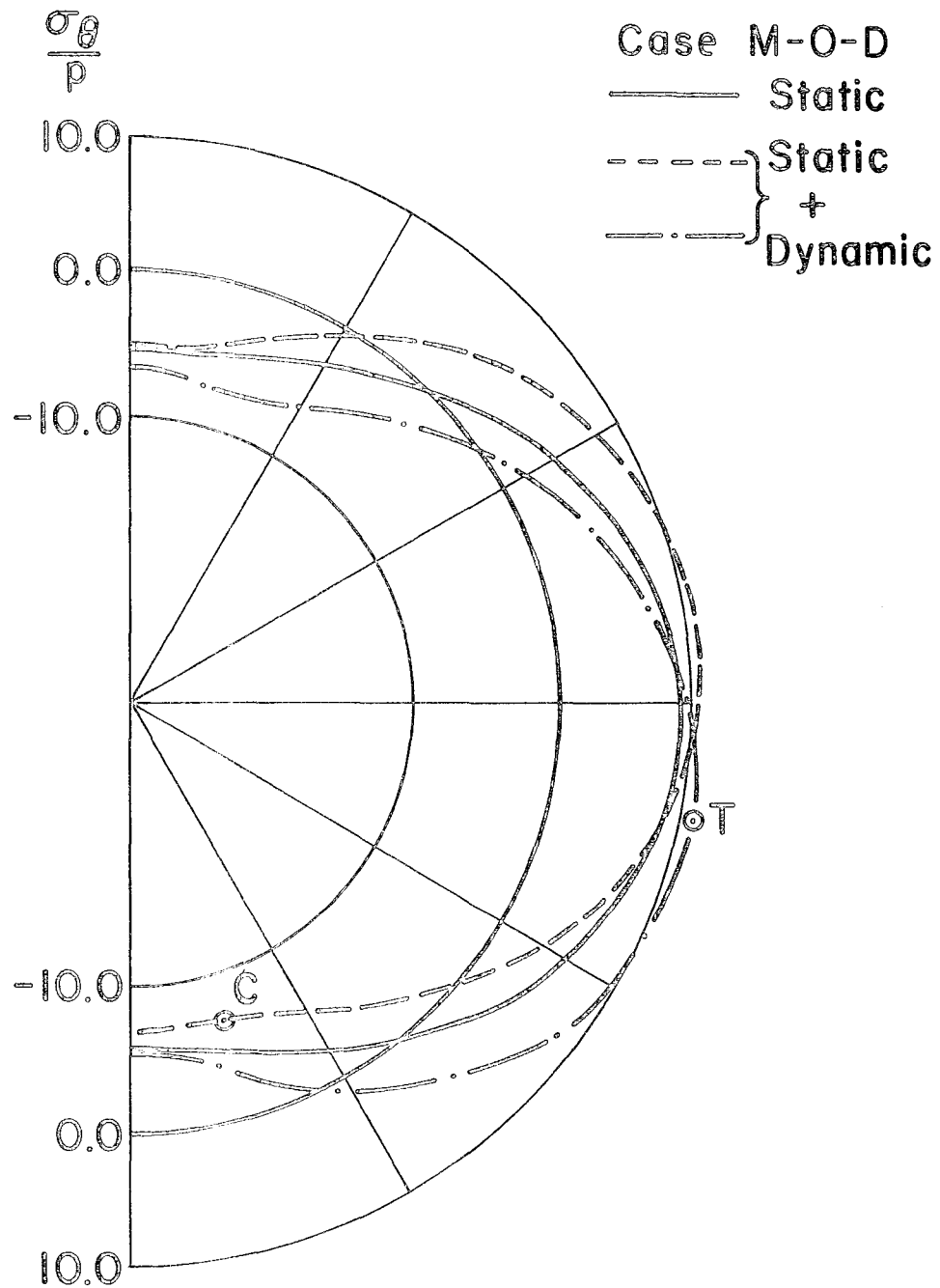


Figure 15. Total Stresses at the Inner Face of the Pipe for the Load Case M-O-D for Horizontal and Vertical Accelerations at 1.12 and 0.64 Sec., Respectively

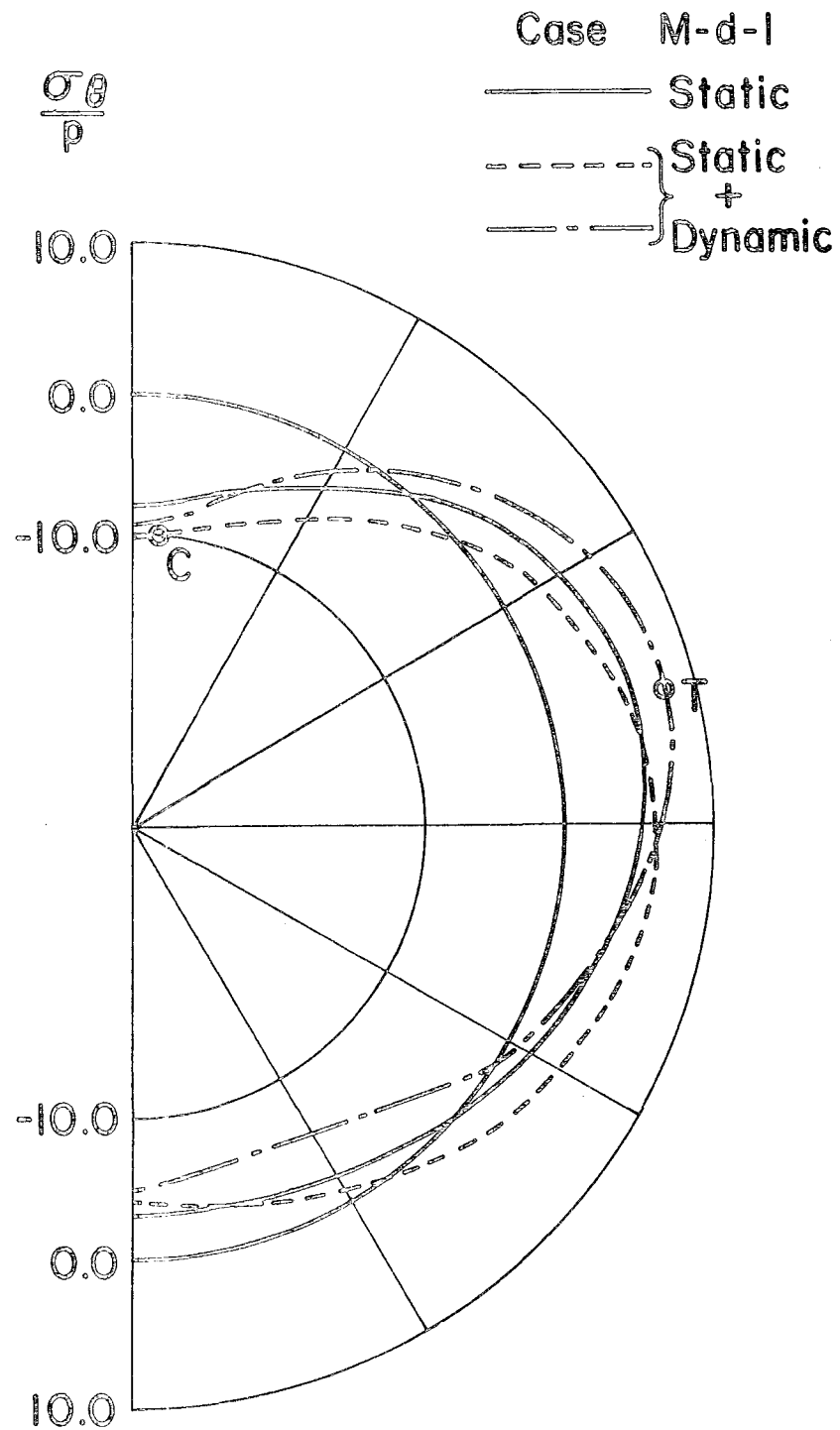


Figure 16. Total Stresses at the Outer Face of the Pipe for the Load Case M-d-I for Horizontal and Vertical Accelerations at 0.64 Sec.

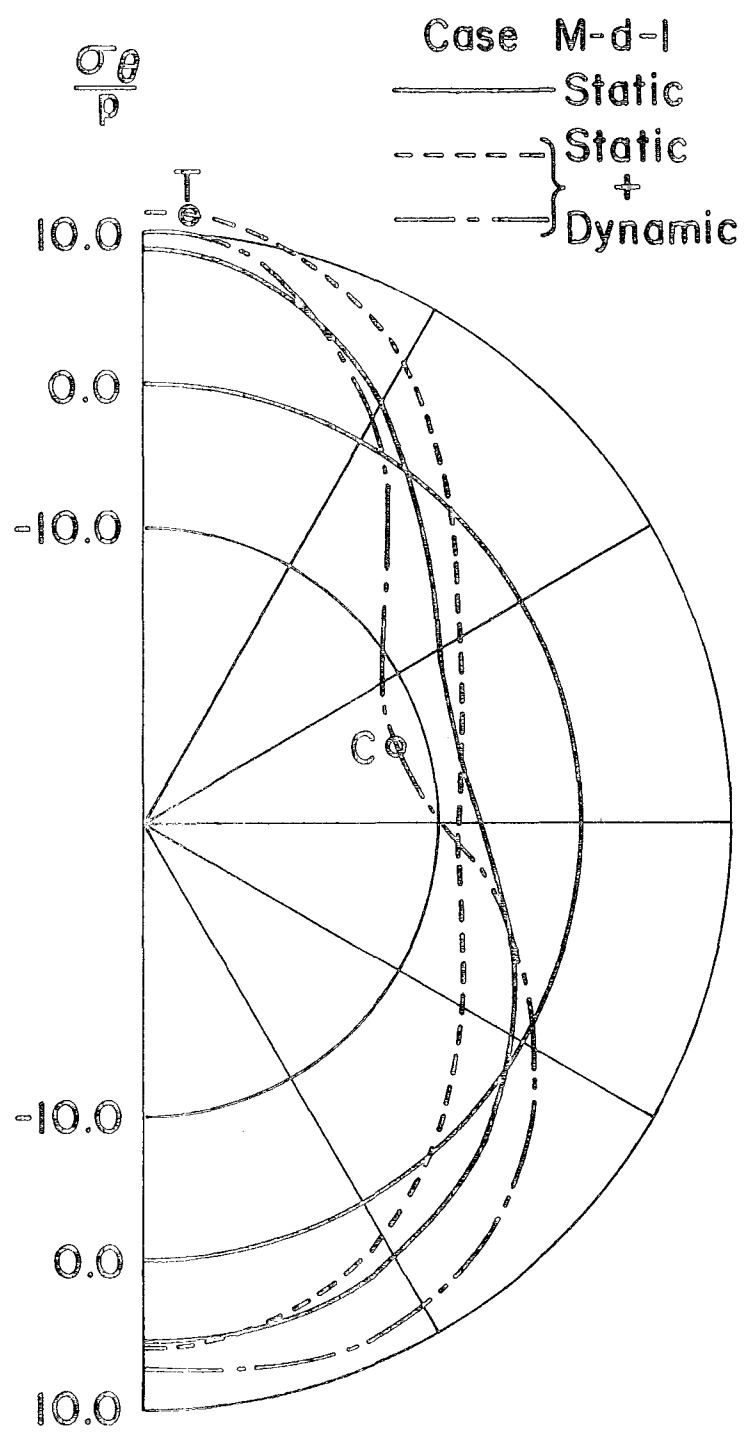


Figure 17. Total Stresses at the Inner Face of the Pipe for the Load Case M-d-I for Horizontal and Vertical Accelerations at 0.64 Sec.

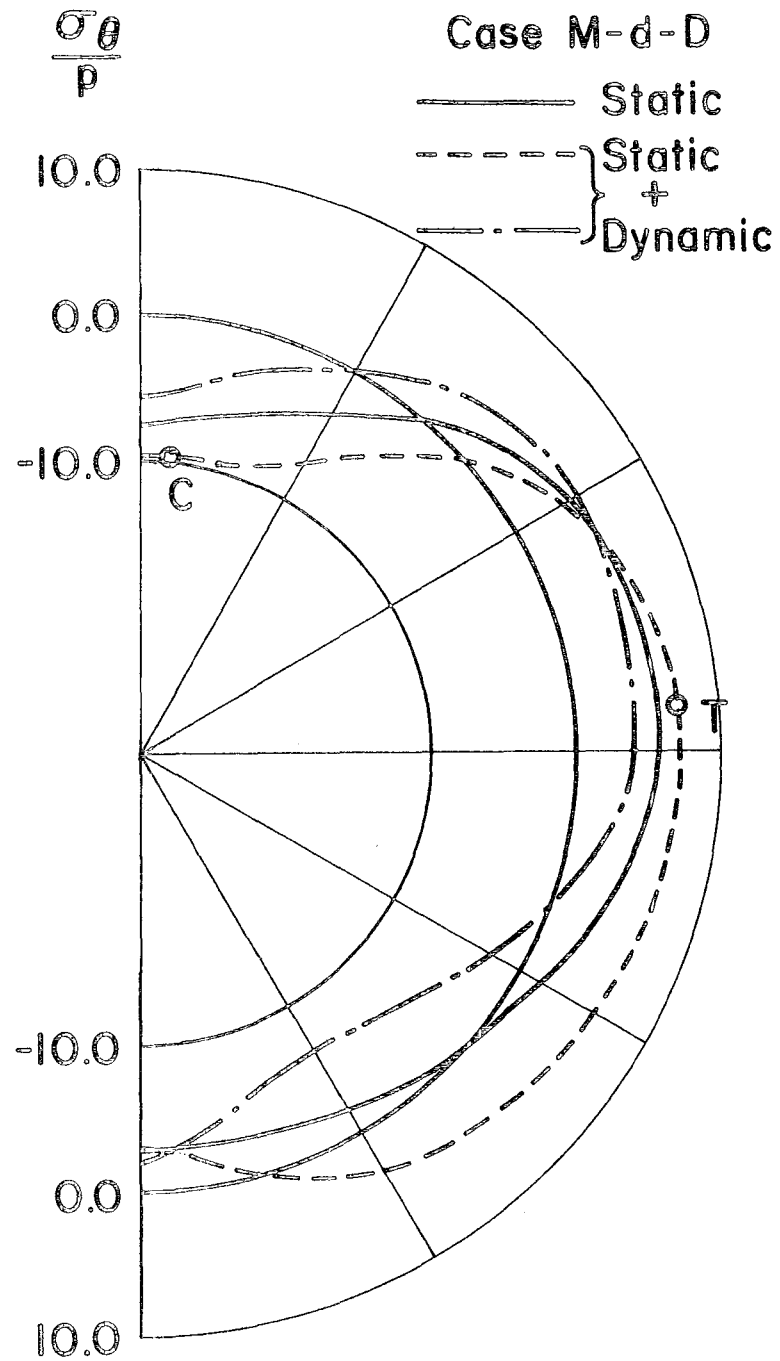


Figure 18. Total Stresses at the Outer Face of the Pipe for the Load Case M-d-D for Horizontal and Vertical Accelerations at 1.28 and 1.12 Sec., Respectively

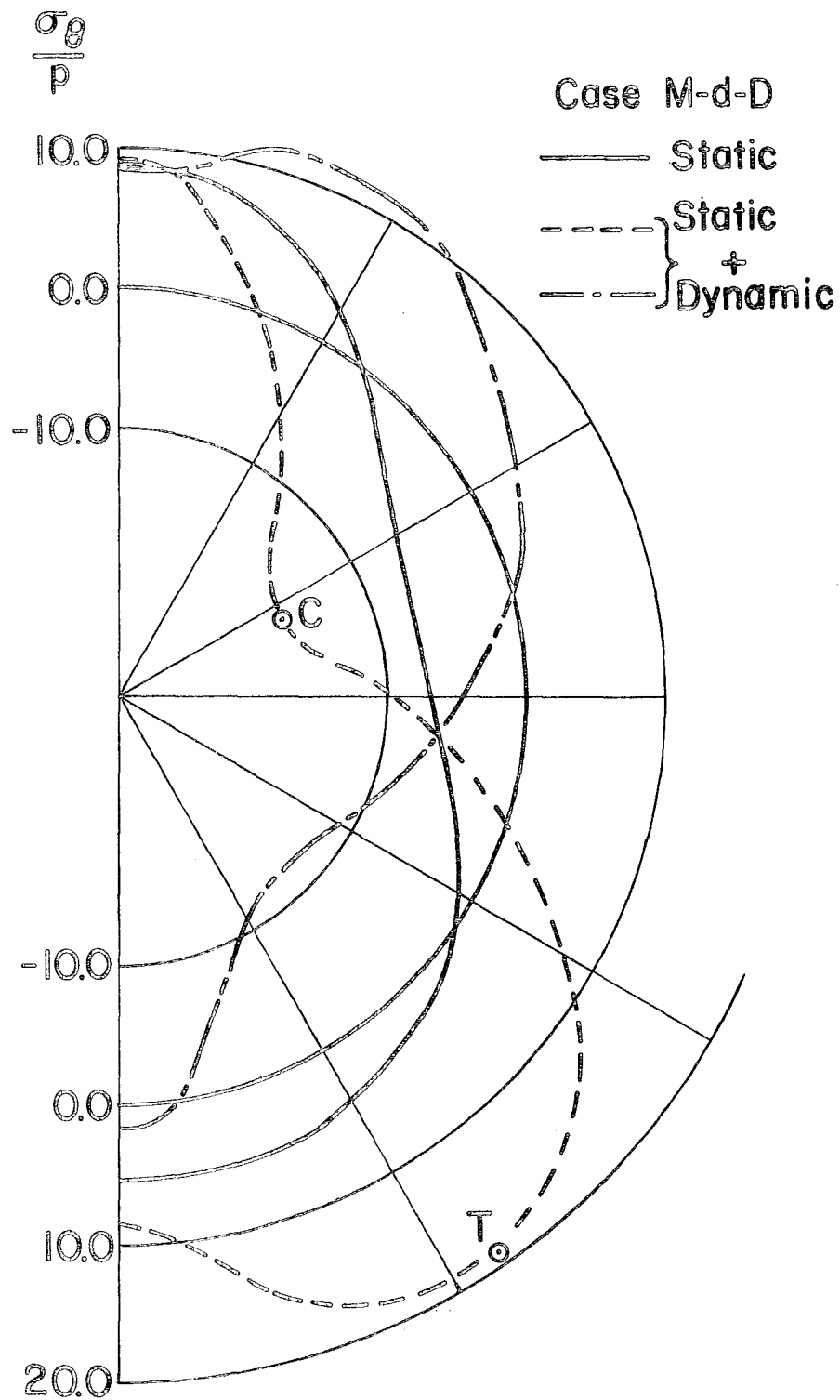


Figure 19. Total Stresses at the Inner Face of the Pipe for the Load Case M-d-D for Horizontal and Vertical Accelerations at 1.28 and 1.12 Sec., Respectively

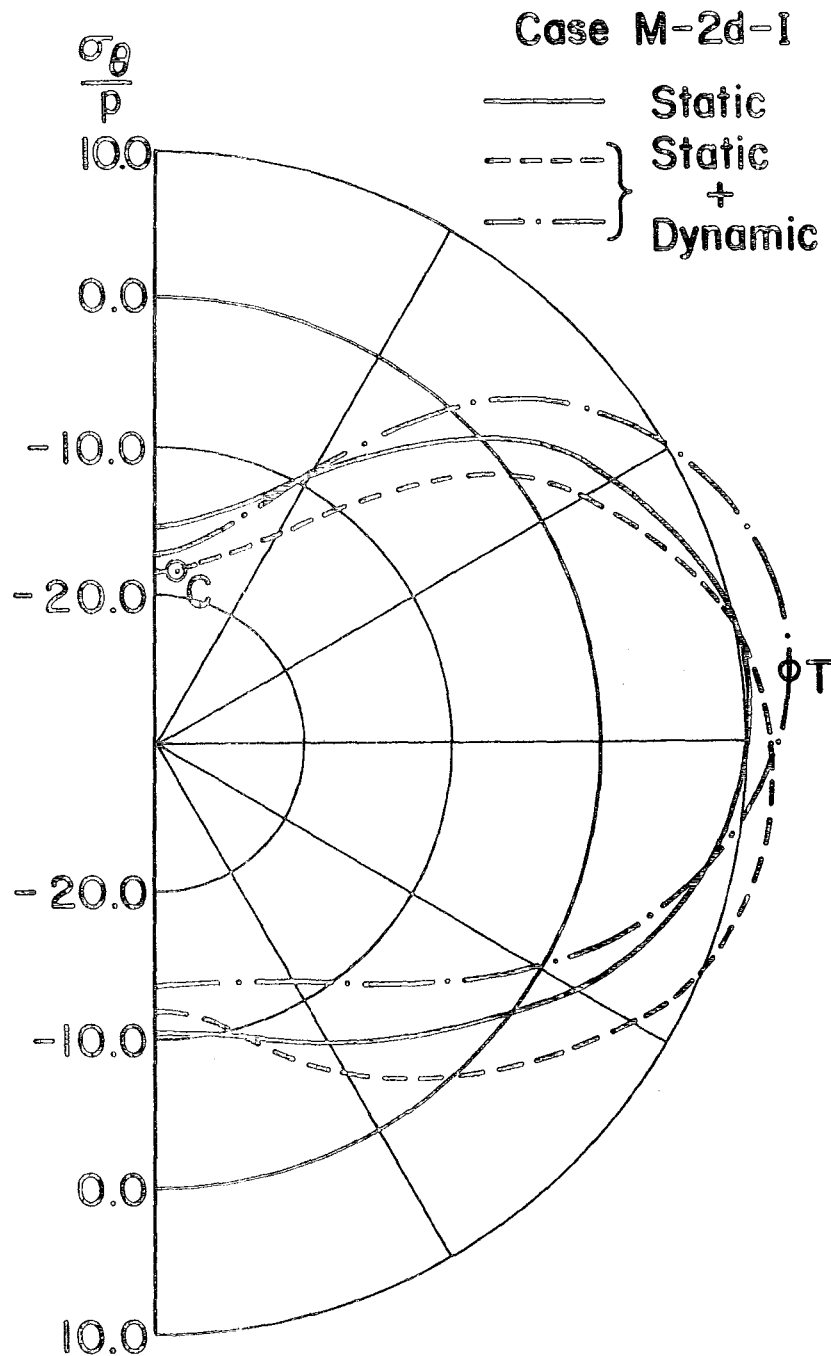


Figure 20. Total Stresses at the Outer Face of the Pipe for the Load Case M-2d-I for Horizontal and Vertical Accelerations at 1.04 and 0.64 Sec., Respectively

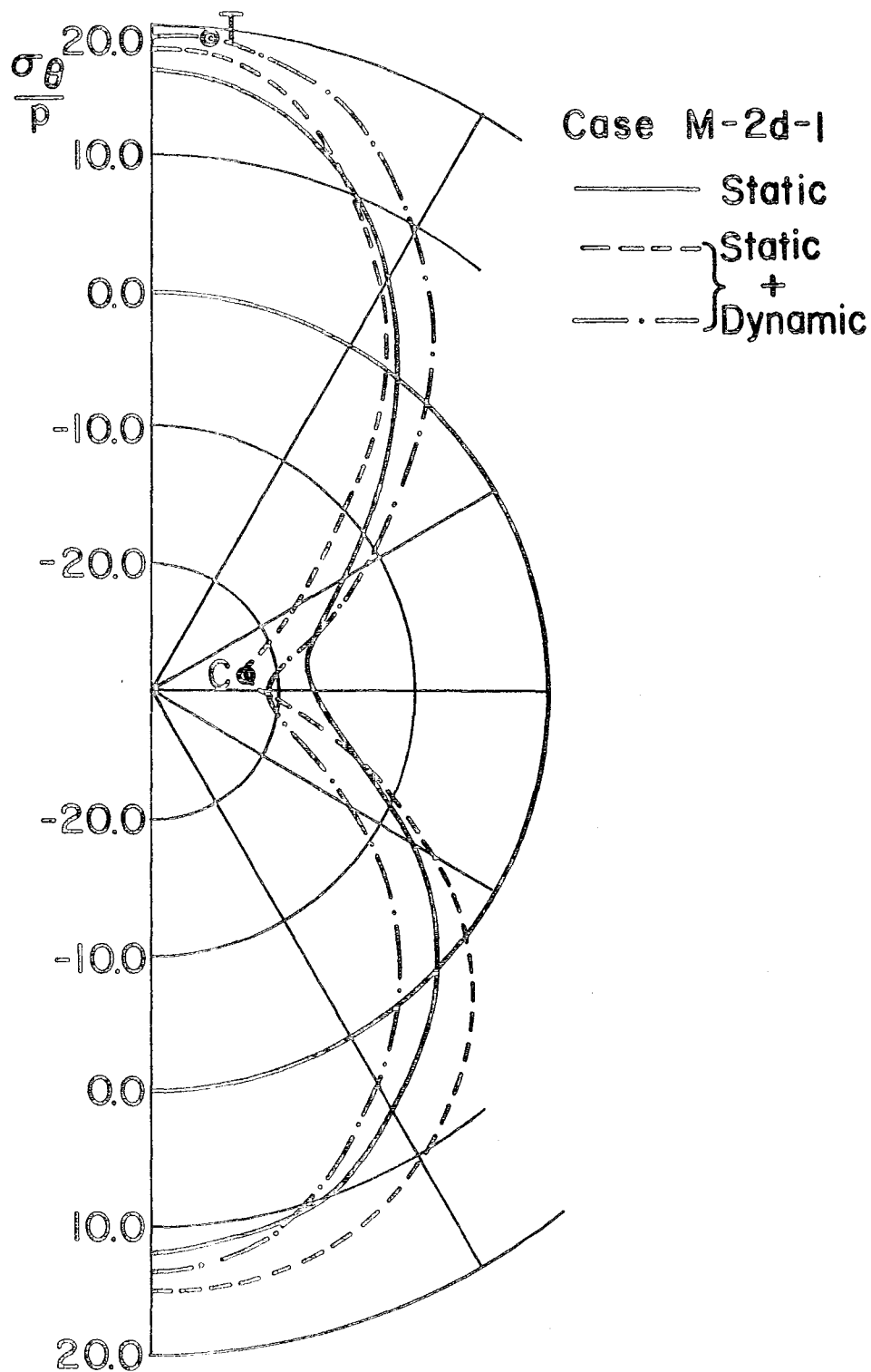


Figure 21. Total Stresses at the Inner Face of the Pipe for the Load Case M-2d-I for Horizontal and Vertical Accelerations at 1.04 and 0.64 Sec., Respectively

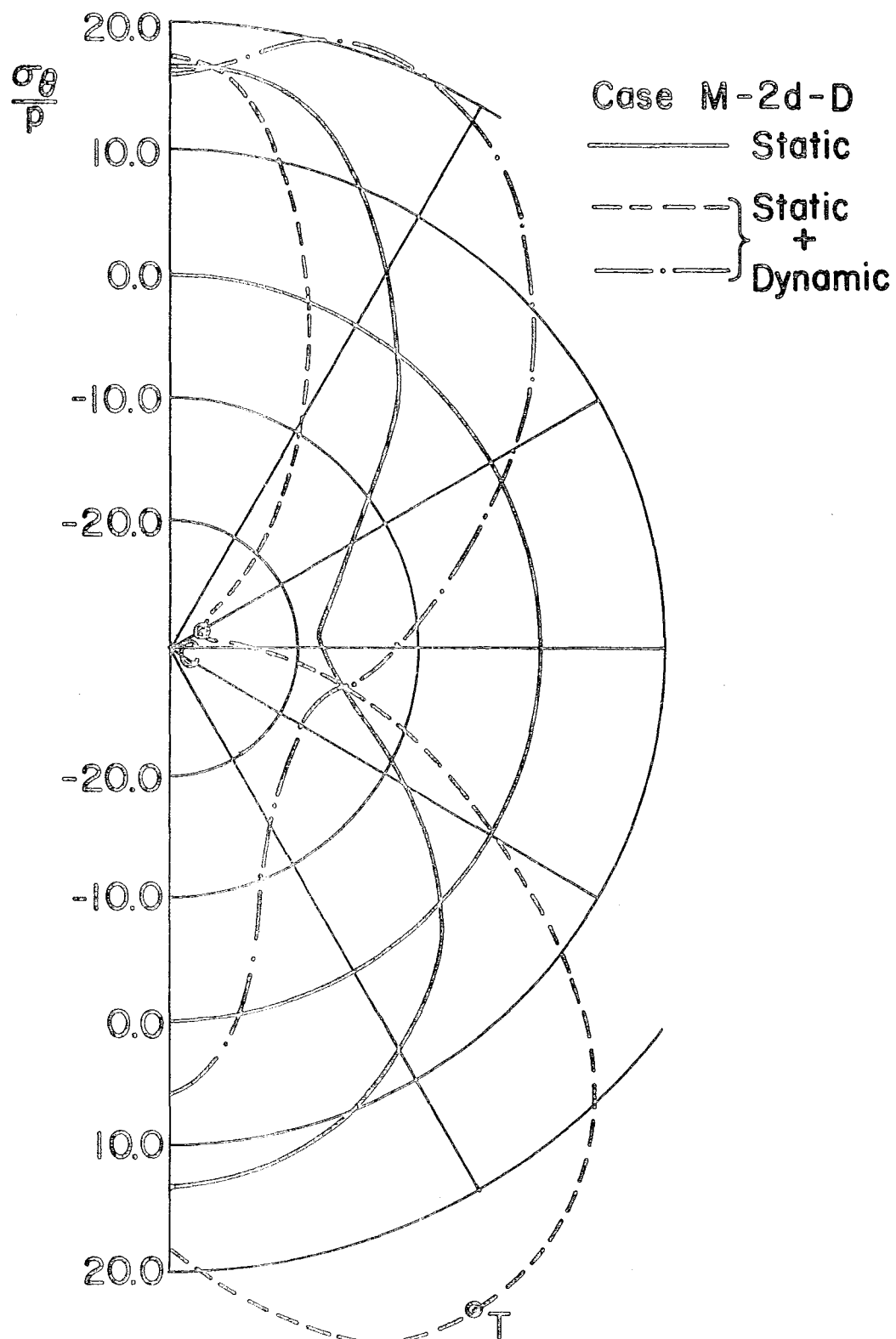


Figure 23. Total Stresses at the Inner Face of the Pipe for the Load Case M-2d-D for Horizontal and Vertical Accelerations at 1.28 and 1.12 Sec., Respectively

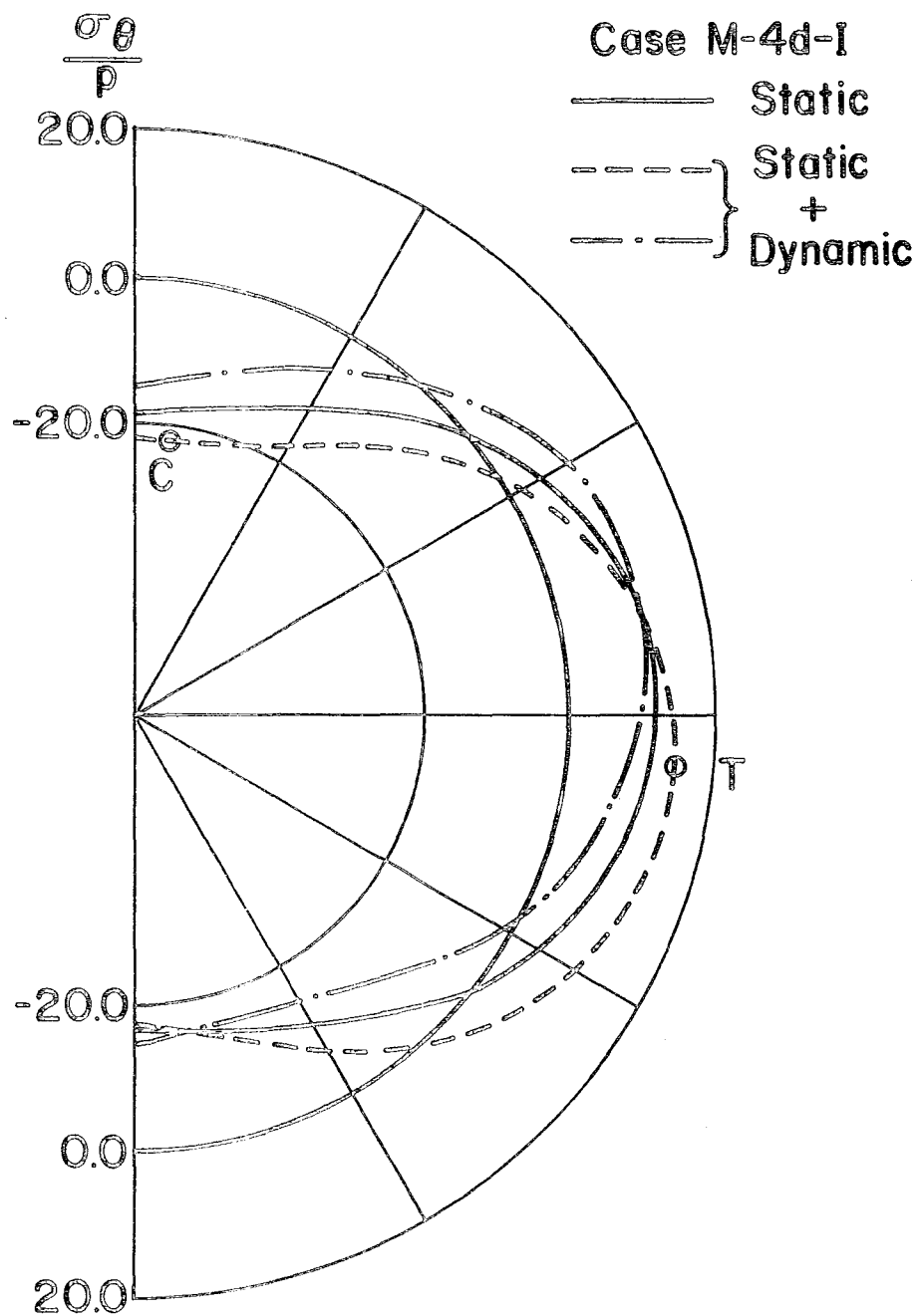


Figure 24. Total Stresses at the Outer Face of the Pipe for the Load Case M-4d-I for Horizontal and Vertical Accelerations at 1.12 and 0.72 Sec., Respectively

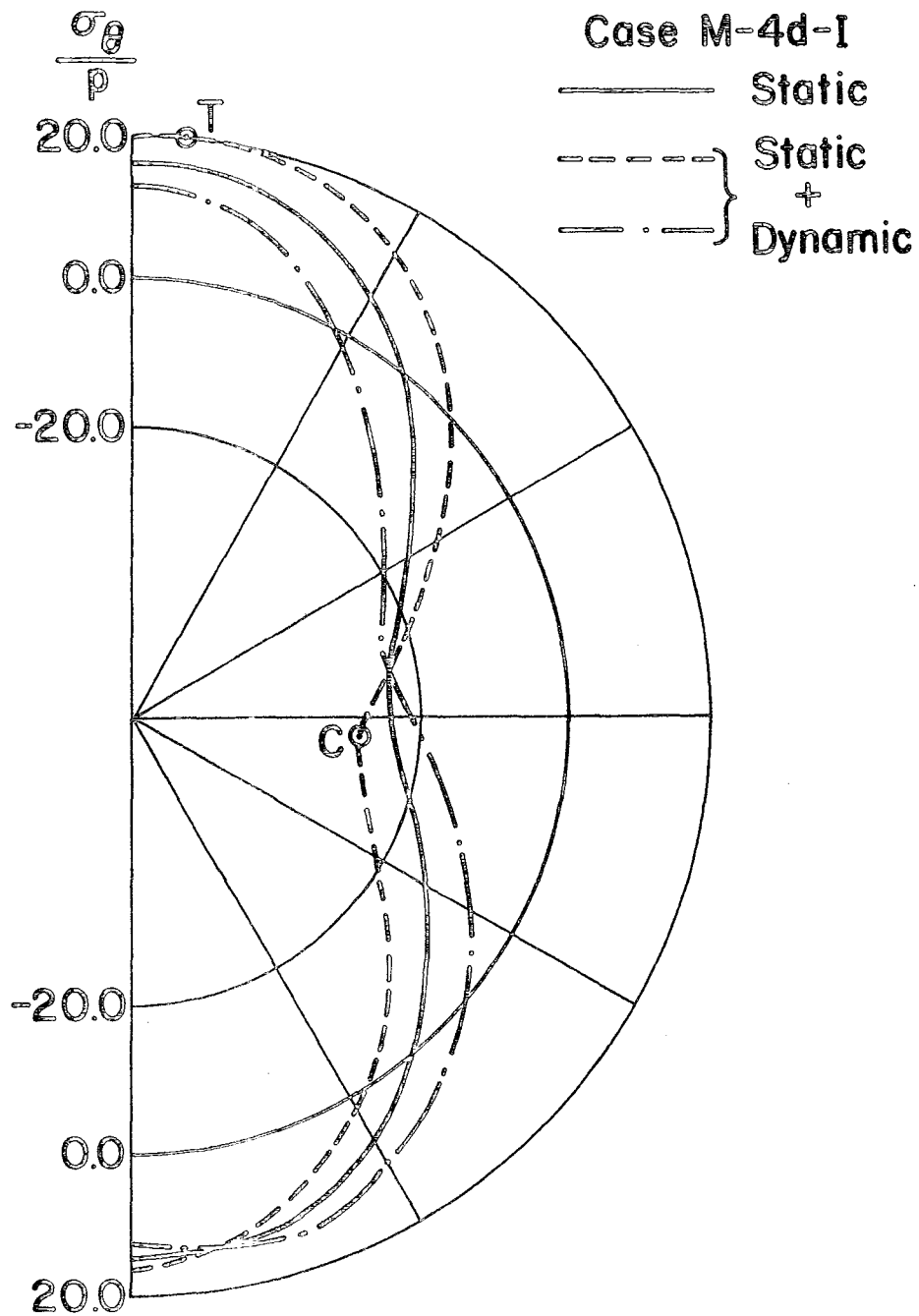


Figure 25. Total Stresses at the Inner Face of the Pipe for the Load Case M-4d-I for Horizontal and Vertical Accelerations at 1.12 and 0.72 Sec., Respectively

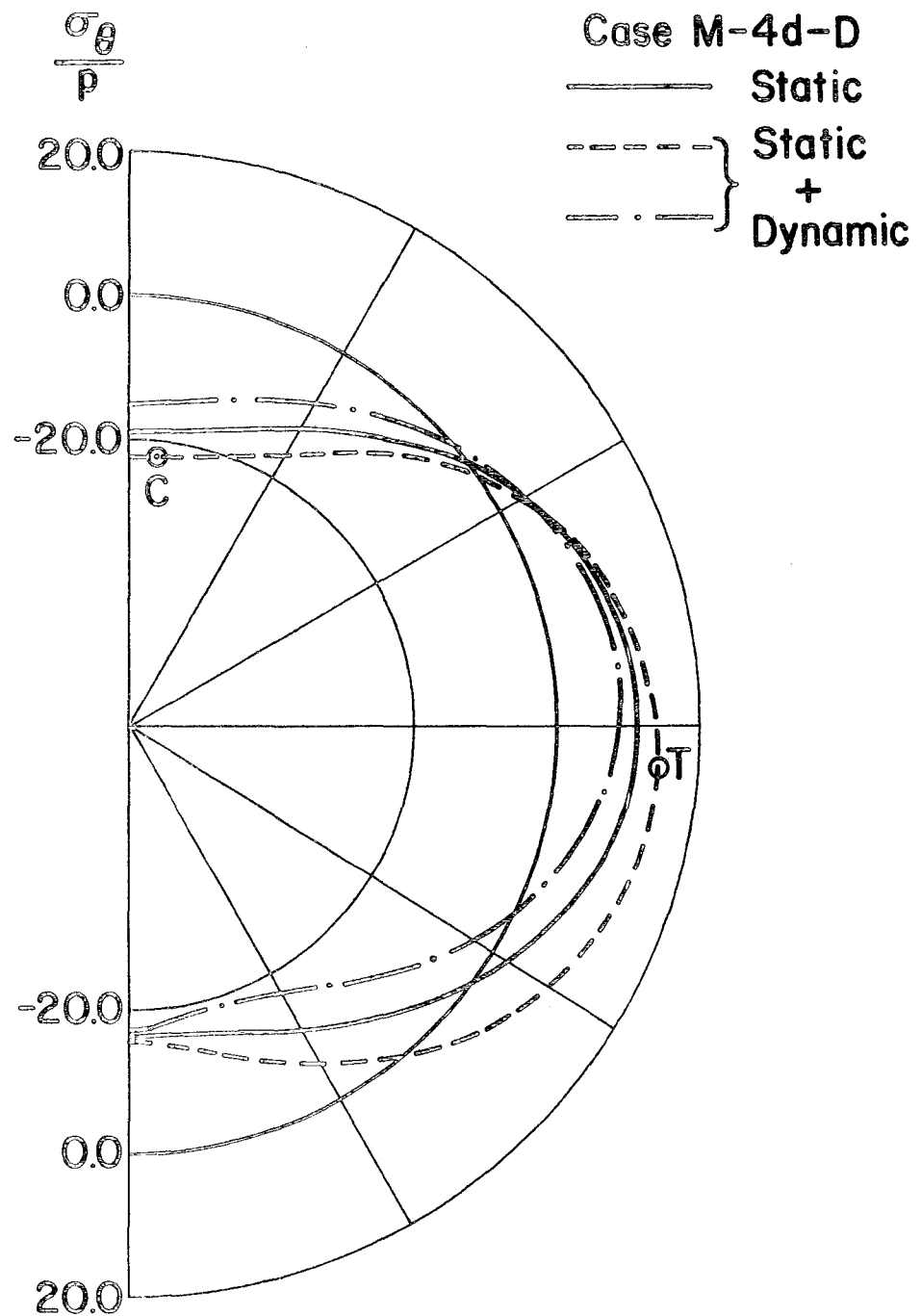


Figure 26. Total Stresses at the Outer Face of the Pipe for the Load Case M-4d-D for Horizontal and Vertical Accelerations at 0.96 and 1.28 Sec., Respectively

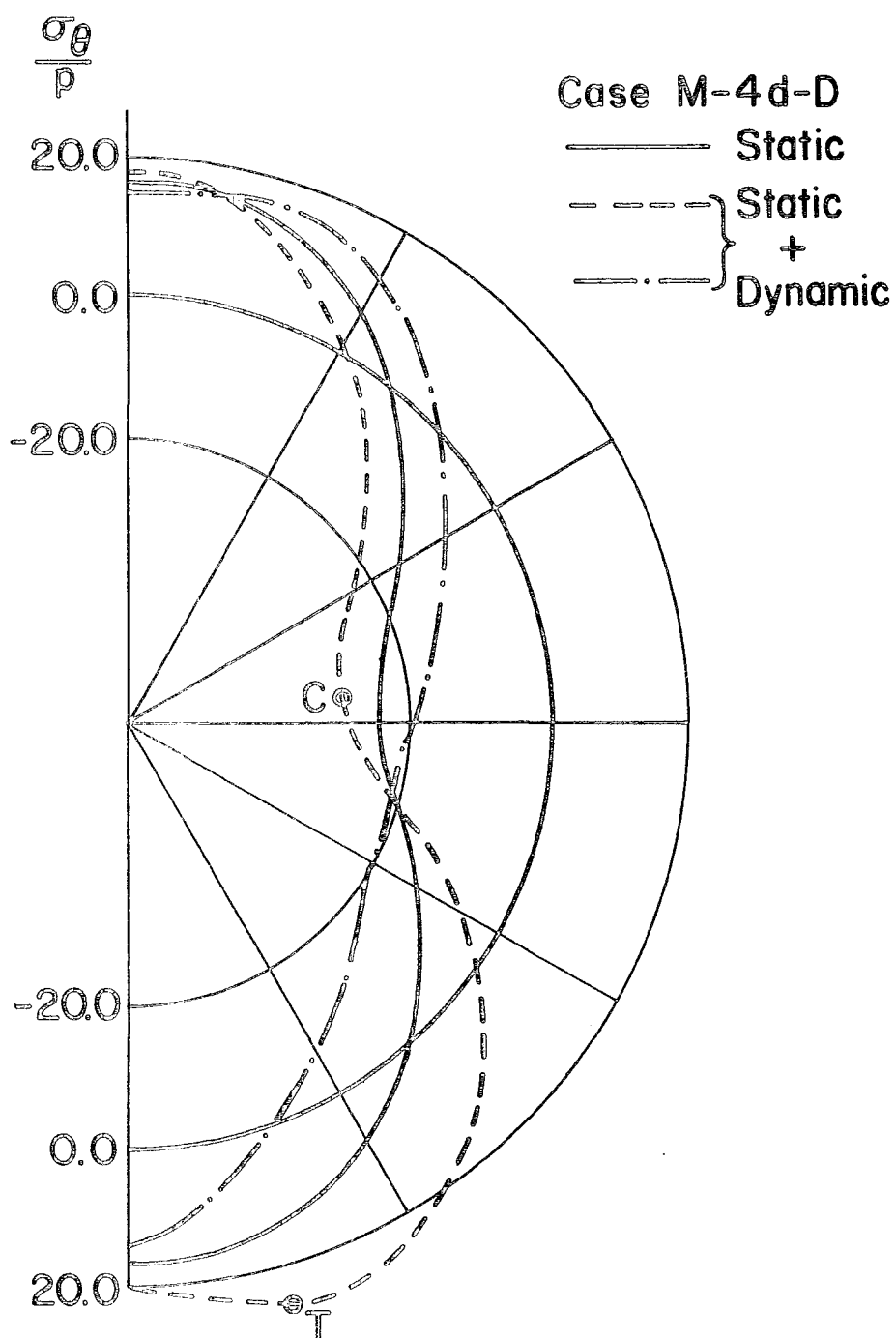


Figure 27. Total Stresses at the Inner Face of the Pipe for the Load Case M-4d-D for Horizontal and Vertical Accelerations at 0.96 and 1.28 Sec., Respectively

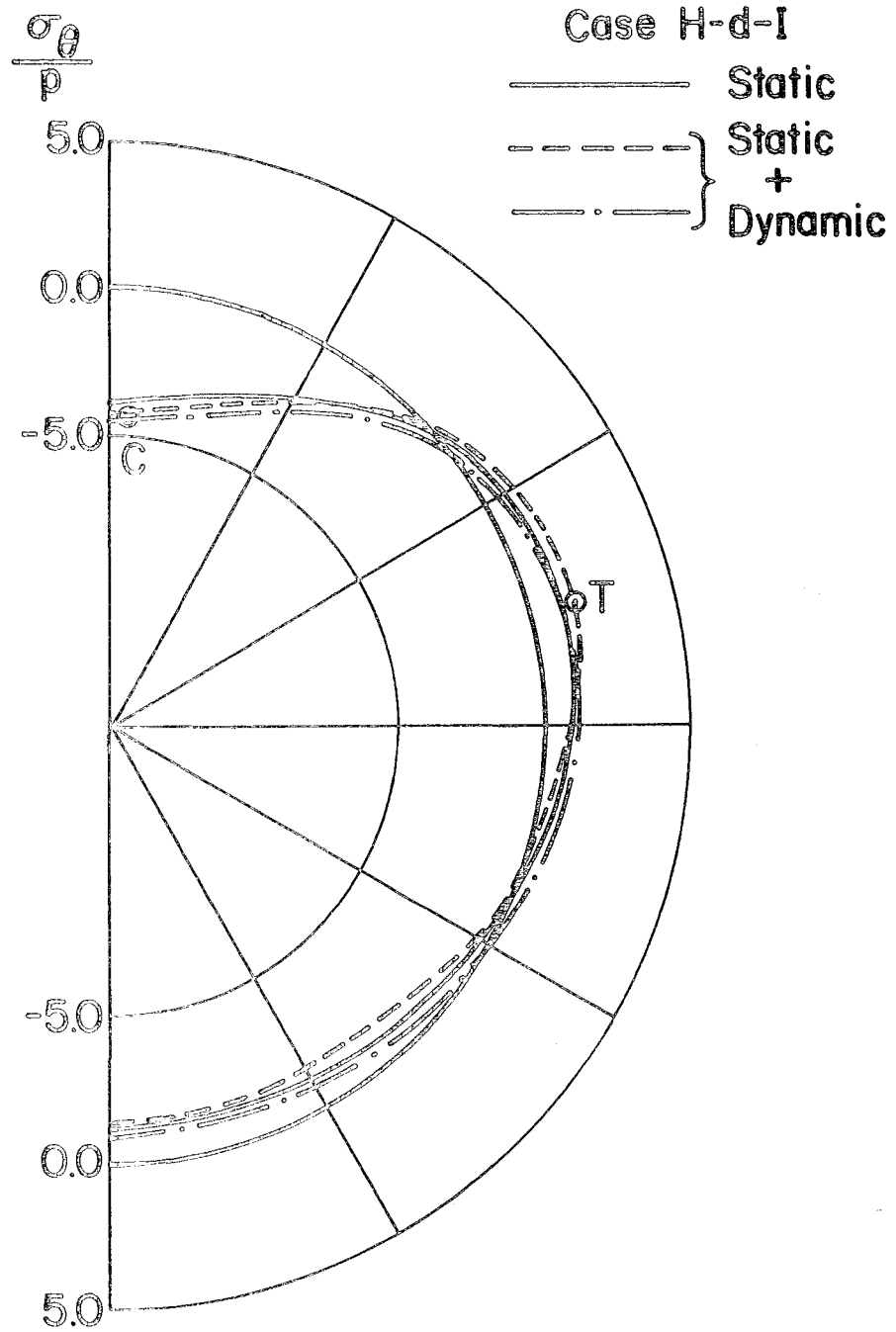


Figure 28. Total Stresses at the Outer Face of the Pipe for the Load Case H-d-I for Horizontal and Vertical Accelerations at 0.56 and 0.64 Sec., Respectively

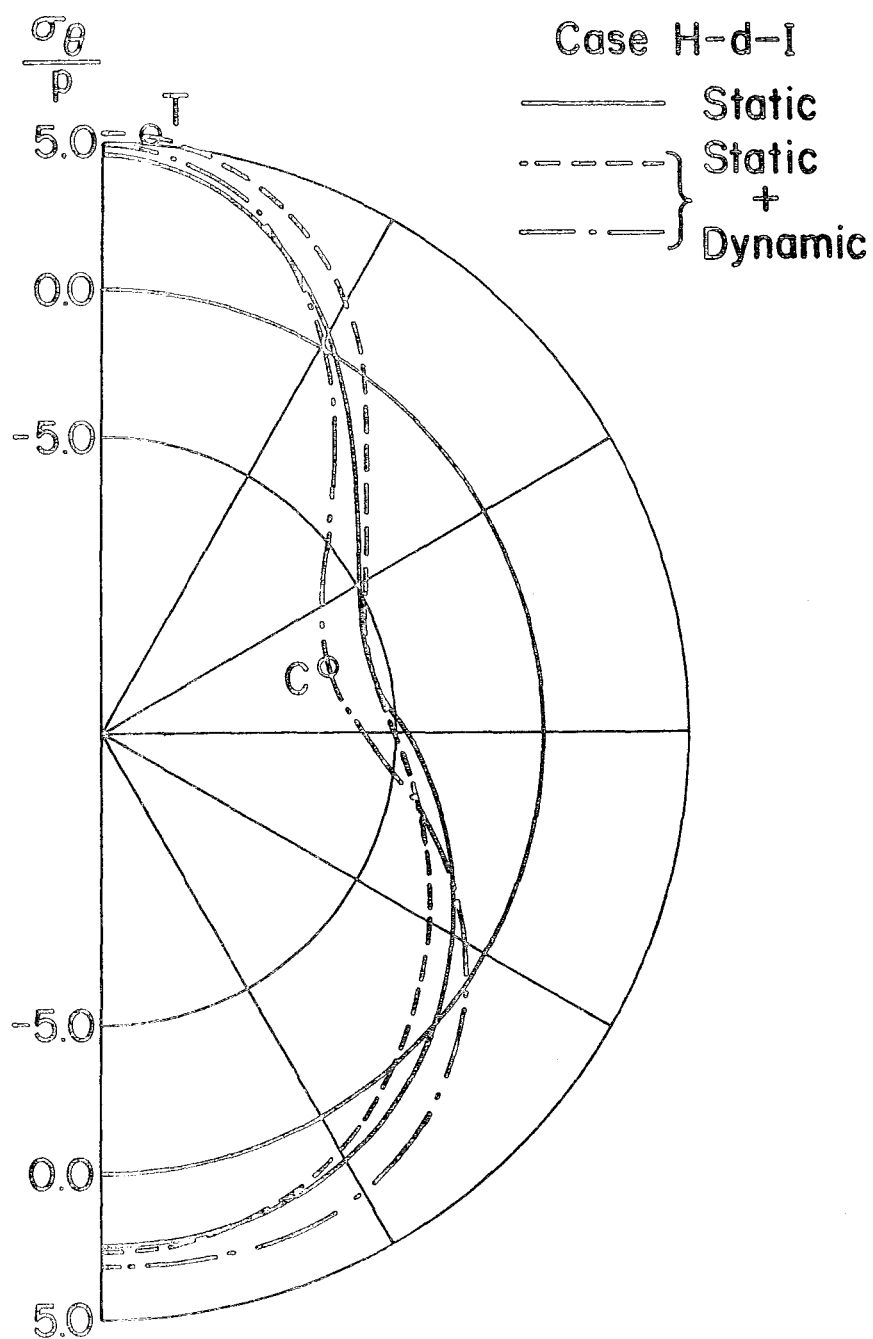


Figure 29. Total Stresses at the Inner Face of the Pipe for the Load Case H-d-I for Horizontal and Vertical Accelerations at 0.56 and 0.64 Sec., Respectively

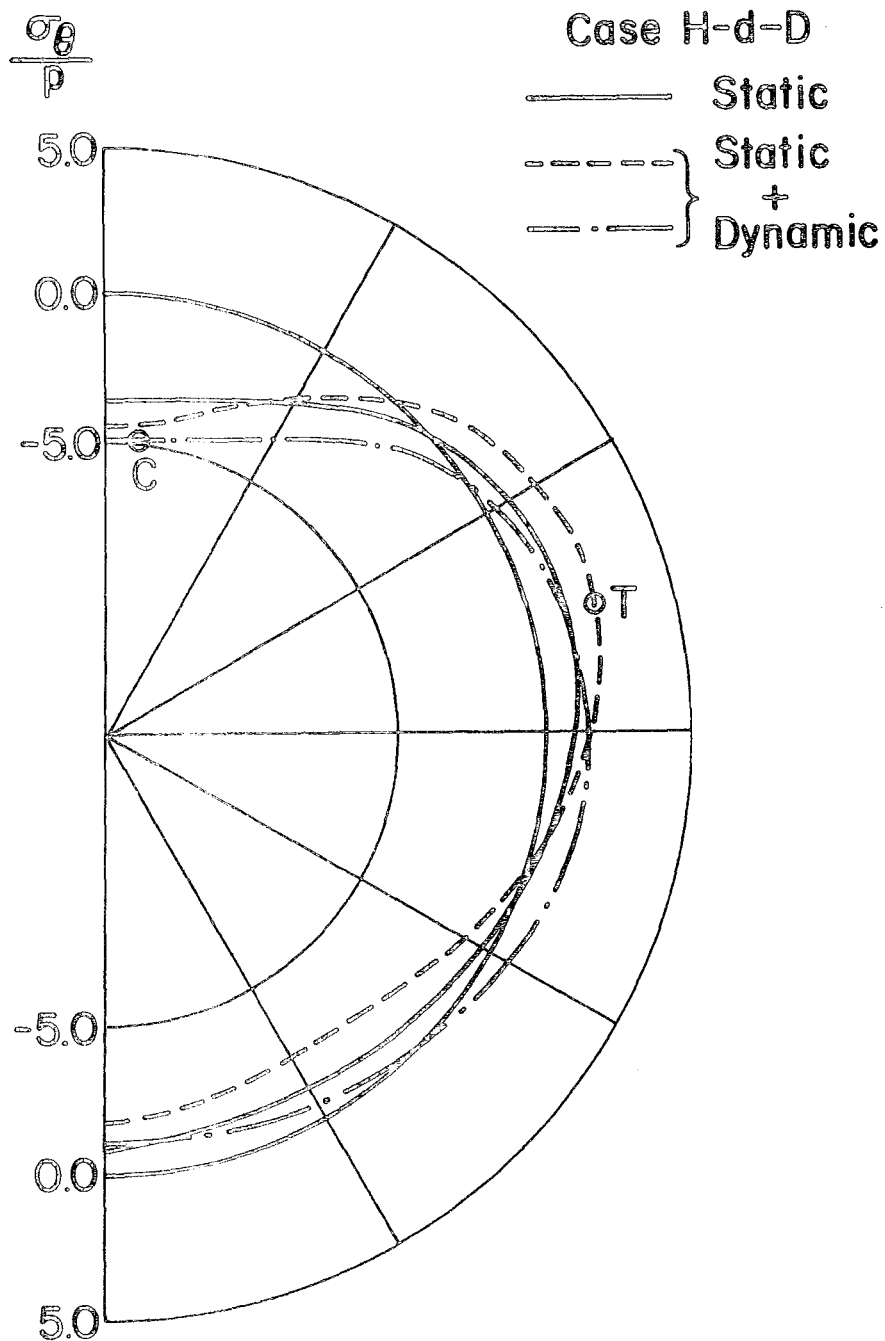


Figure 30. Total Stresses at the Outer Face of the Pipe for the Load Case H-d-D for Horizontal and Vertical Accelerations at 0.64 and 0.56 Sec., Respectively

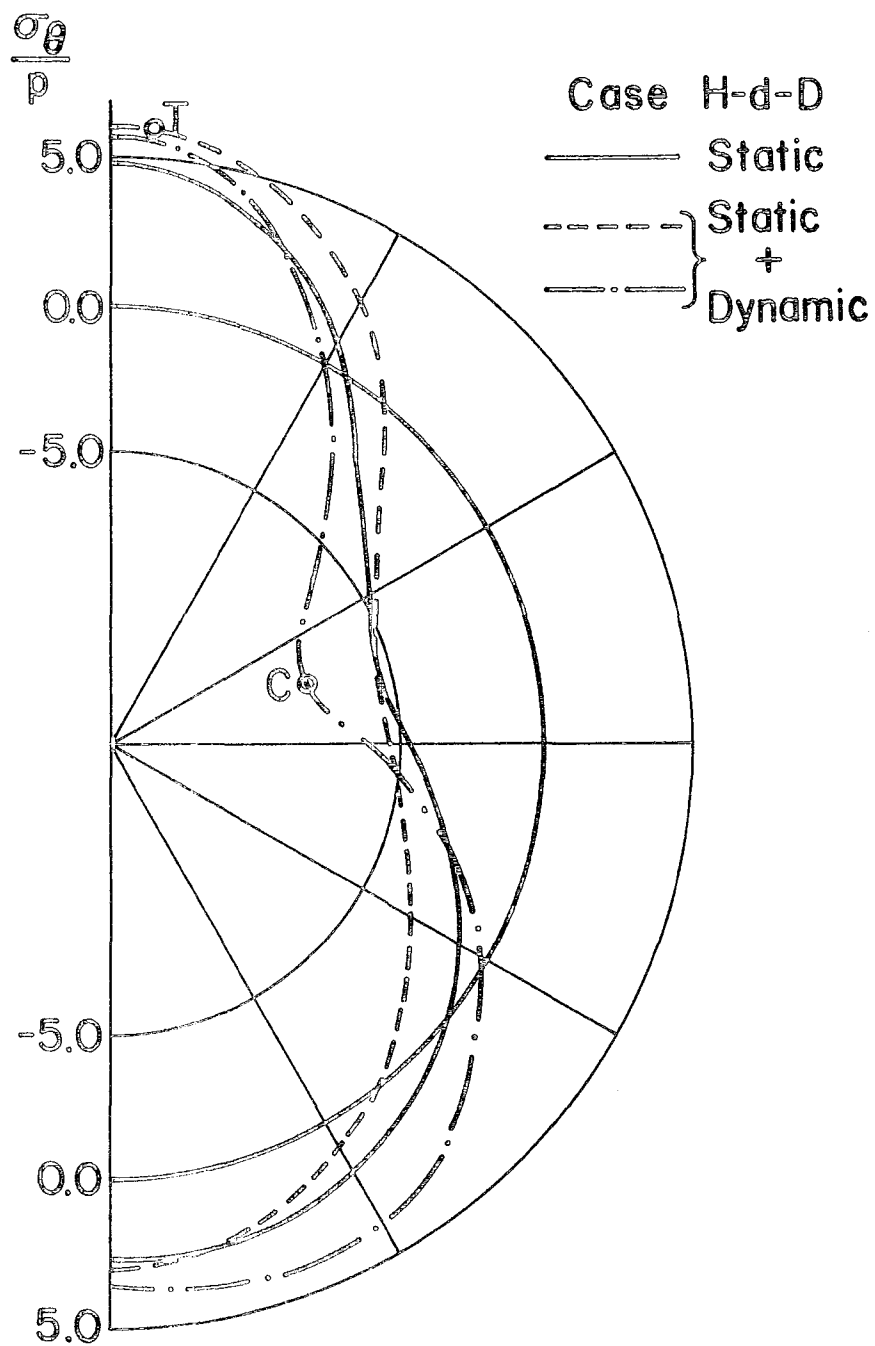


Figure 31. Total Stresses at the Inner Face of the Pipe for the Load Case H-d-D for Horizontal and Vertical Accelerations at 0.64 and 0.56 Sec., Respectively

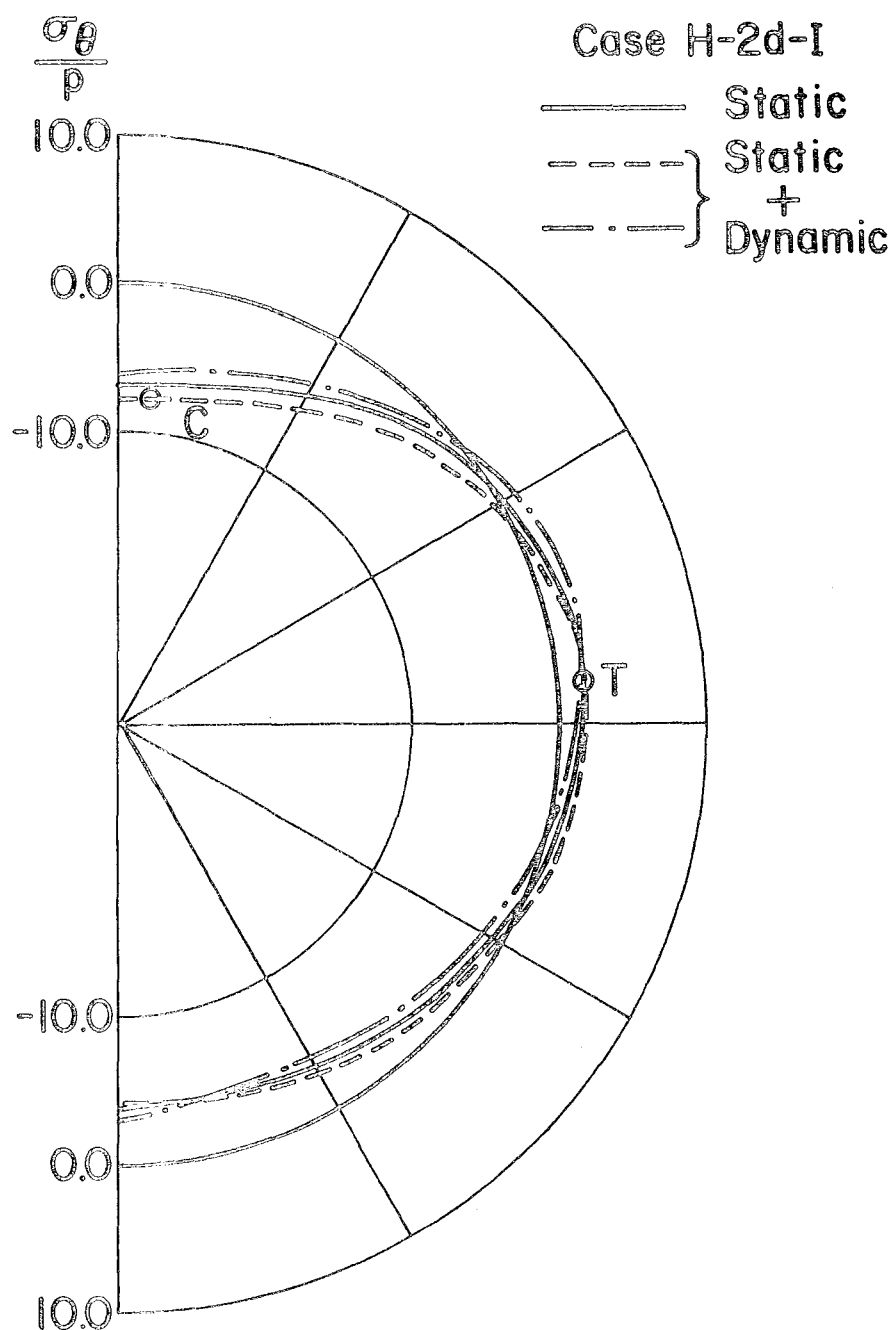


Figure 32. Total Stresses at the Outer Face of the Pipe for the Load Case H-2d-I for Horizontal and Vertical Accelerations at 0.64 and 0.56 Sec., Respectively

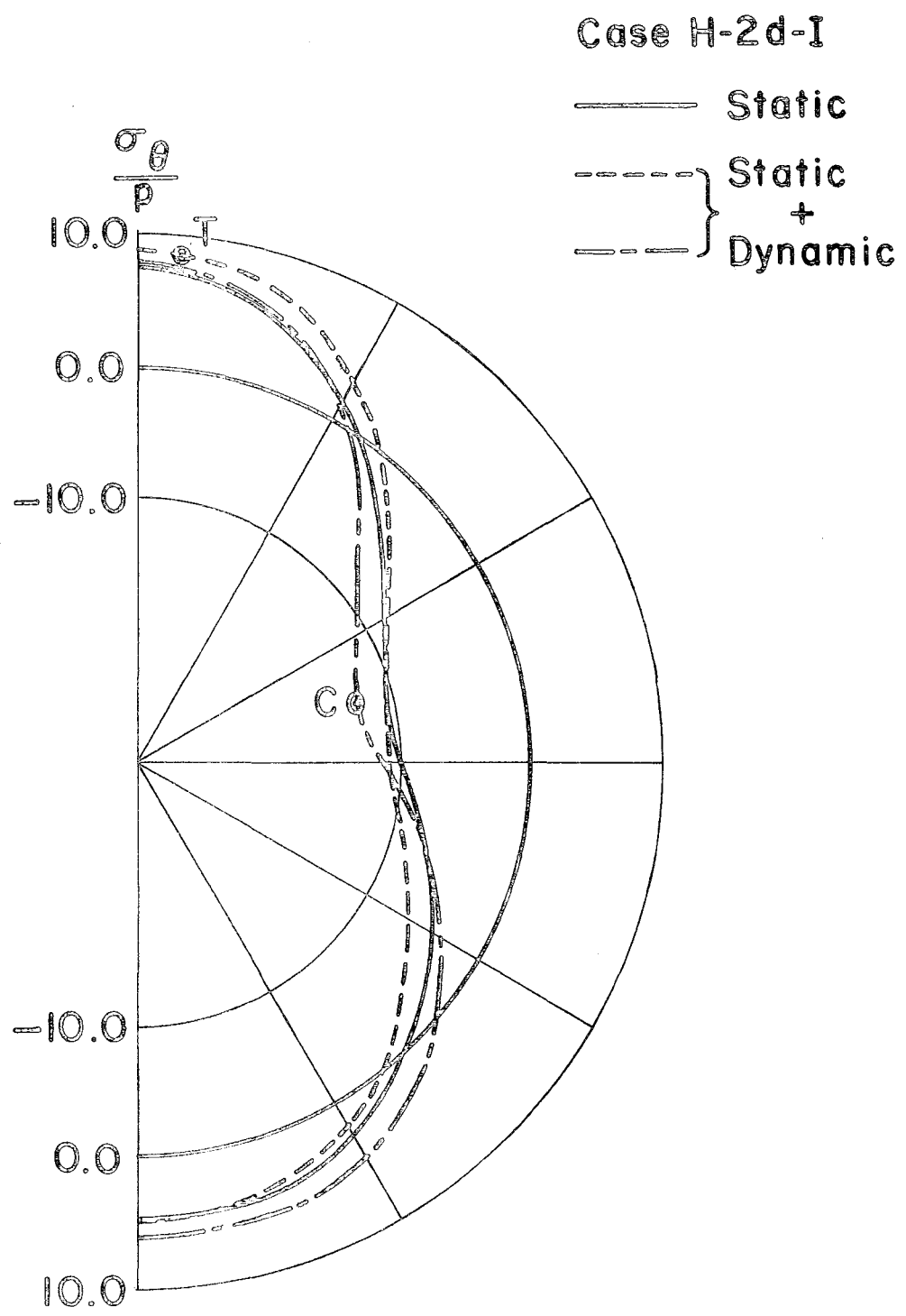


Figure 33. Total Stresses at the Inner Face of the Pipe for the Load Case H-2d-I for Horizontal and Vertical Accelerations at 0.64 and 0.56 Sec., Respectively

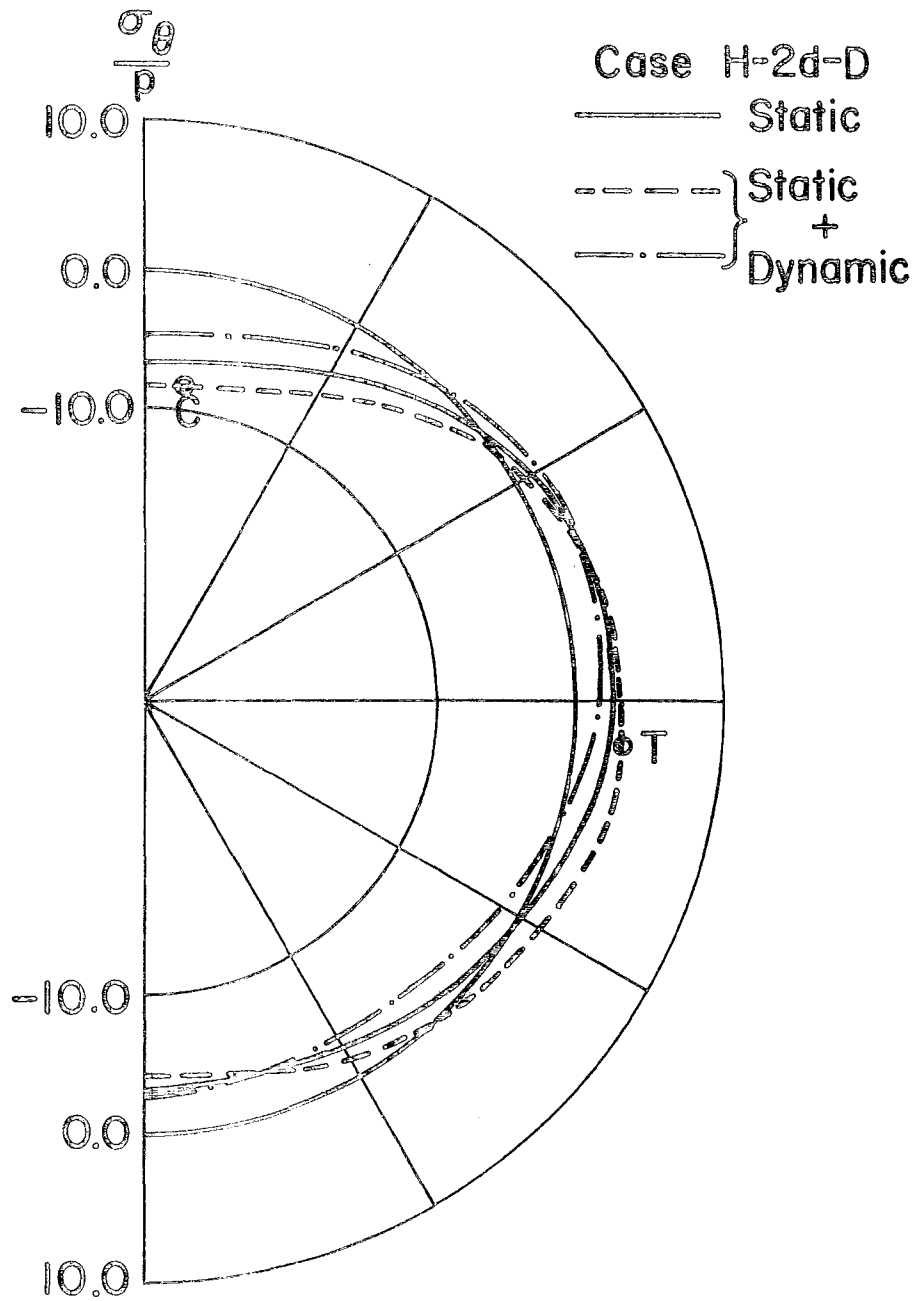


Figure 34. Total Stresses at the Outer Face of the Pipe for the Load Case H-2d-D for Horizontal and Vertical Accelerations at 0.64 and 1.04 Sec., Respectively

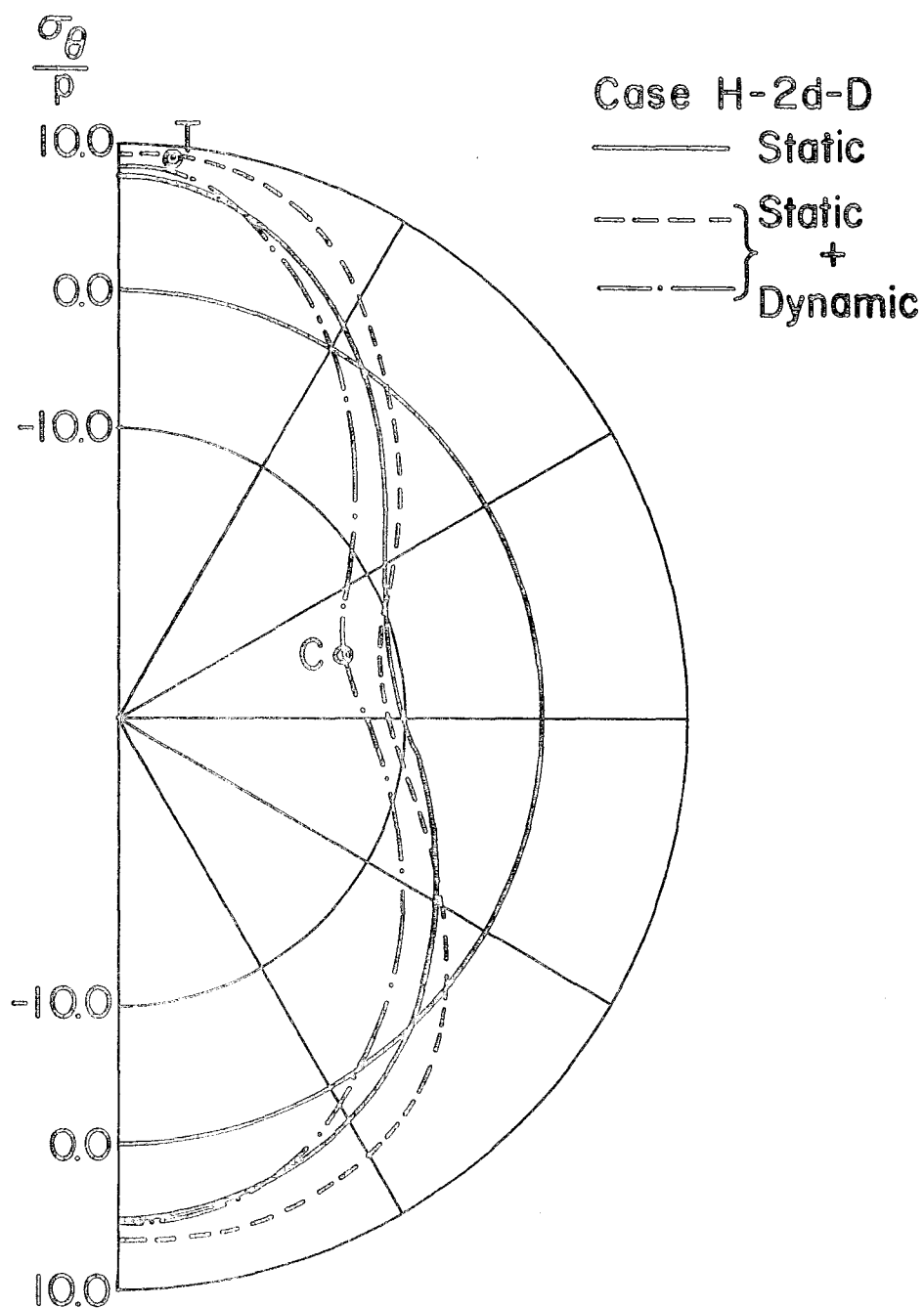


Figure 35. Total Stresses at the Inner Face of the Pipe for the Load Case H-2d-D for Horizontal and Vertical Accelerations at 0.64 and 1.04 Sec., Respectively

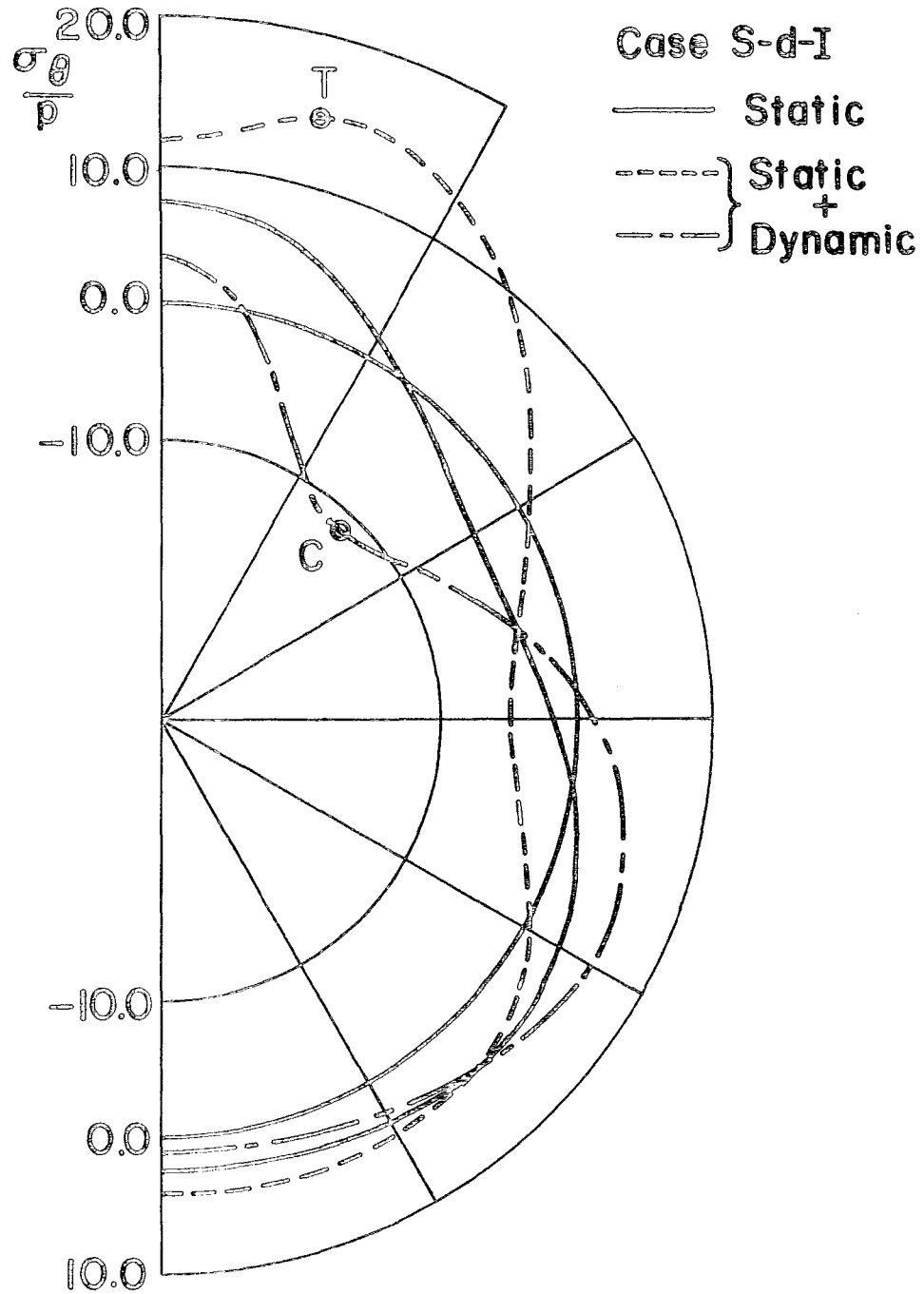


Figure 37. Total Stresses at the Inner Face of the Pipe for the Load Case S-d-I for Horizontal and Vertical Accelerations at 1.76 and 1.04 Sec., Respectively

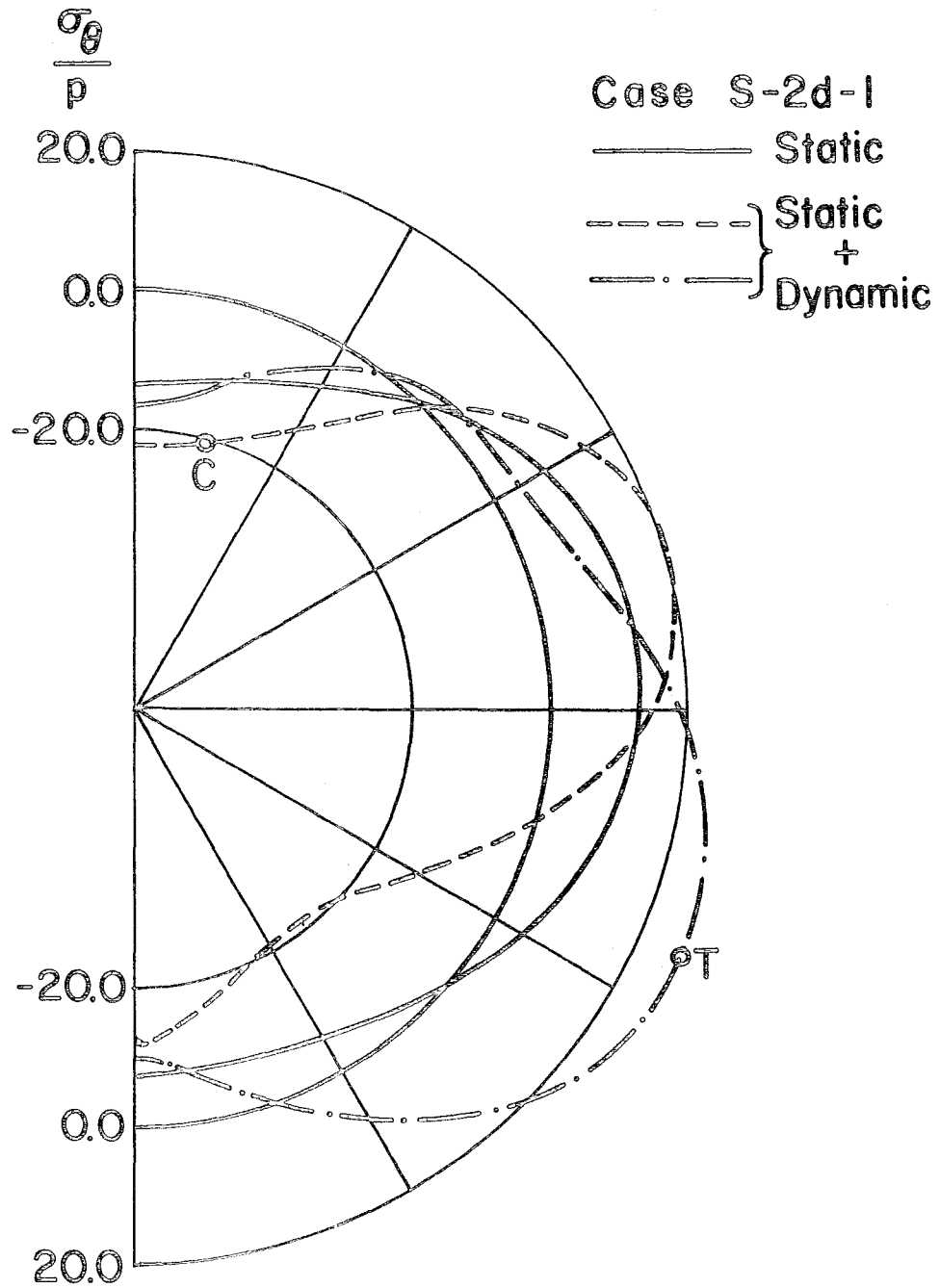


Figure 38. Total Stresses at the Outer Face of the Pipe for the Load Case S-2d-I for Horizontal and Vertical Accelerations at 1.36 and 1.12 Sec., Respectively

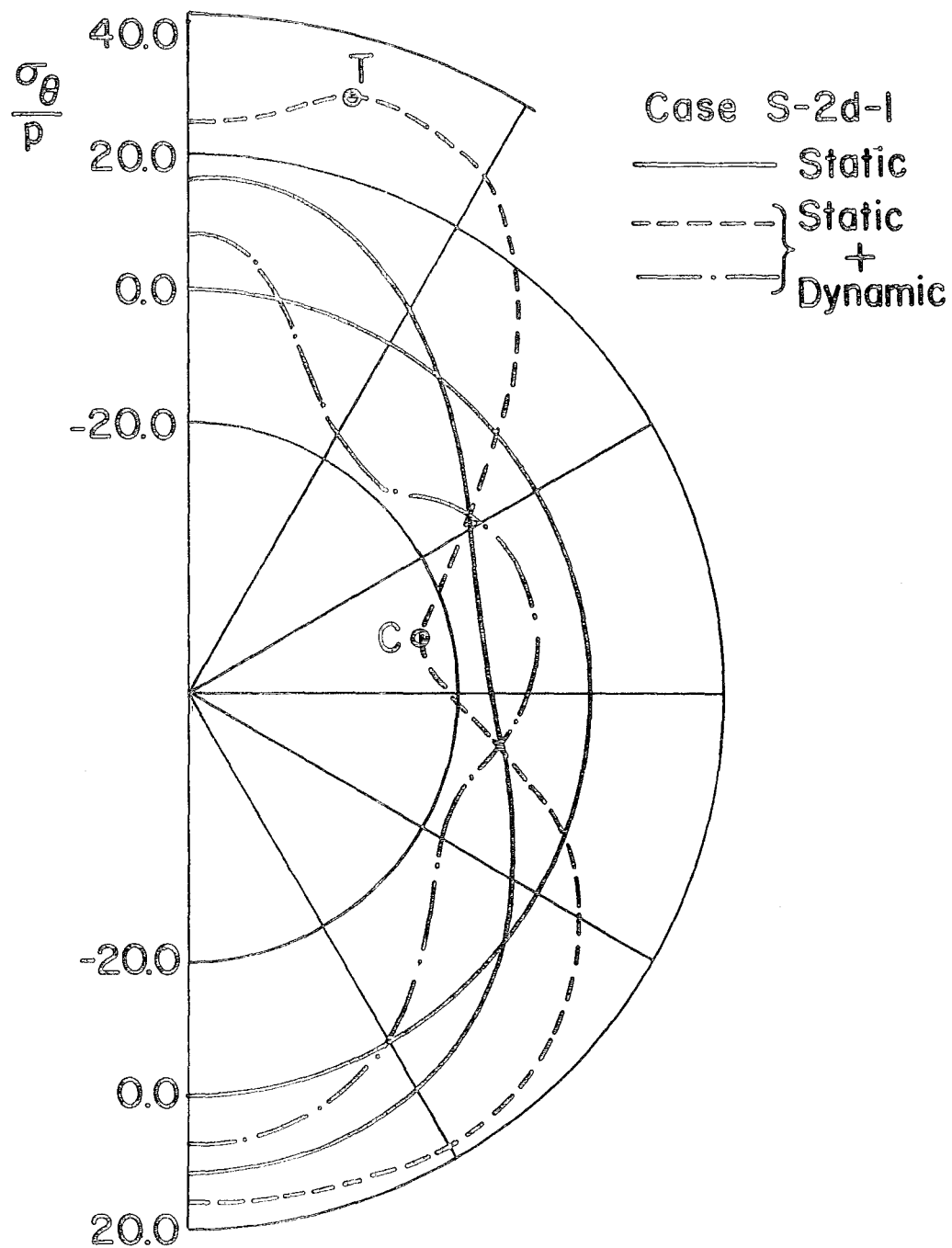


Figure 39. Total Stresses at the Inner Face of the Pipe for the Load Case S-2d-I for Horizontal and Vertical Accelerations at 1.36 and 1.12 Sec., Respectively

outside fibers of the pipe thickness are plotted in separate figures. Numerical values of non-dimensional stresses at these points for all load cases are tabulated in Table 3 for outer and inner faces of the pipe. The maximum total stress divided by the maximum static stress, for a given load case, gives the Dynamic Load Factor (DLF). Dynamic load factors for all load cases are obtained for compressive and tensile stresses on each face of the pipe and are tabulated in Table 4.

Effect of Variable Load Width on Pipe Stresses

Effect of variable surface load widths on stresses in a pipe was sought for the types of soils considered in Table 1. As mentioned earlier, medium and hard soils were analyzed for strain-independent as well as strain-compatible soil properties while strain-independent soil properties only were utilized in the analyses with the soft soil.

Strain-Independent Soil Properties

Uniform surface loads of widths d , $2d$ and $4d$ are considered for the medium soil leading to load cases M-d-I, M-2d-I and M-4d-I, respectively. Non-dimensional pipe stresses for these load cases are plotted for outer and inner fibers of the pipe as shown in Figures 16, 17, 20, 21, 24 and 25, and the maximum total compressive and tensile stresses for these cases are given in Table 3.

The maximum total compressive stresses at the inner face of the pipe for load cases M-d-I, M-2d-I and M-4d-I are 12.23, 22.22, and 29.35, respectively; whereas the corresponding dynamic load factors, as shown in Table 4, are 1.51, 1.21, and 1.19. Similarly, the tensile stresses at the inner face of the pipe for cases M-d-I, M-2d-I and M-4d-I are 11.30, 19.30, and 20.40, respectively; and the corresponding dynamic load factors are 1.27, 1.20, and 1.22. It is obvious from these results

Table 3. Non-dimensional Tangential Stresses in pipe for various Load Cases

Load Case		M-0-I	M-0-D	M-d-I	M-d-D	M-2d-I	M-2d-D	M-4d-I	M-4d-D
Outer face Compression at C	Static	3.55	3.08	7.45	7.45	14.91	13.45	18.26	18.26
	Horizontal Acceleration	0.89	1.45	0.54	0.61	0.47	4.01	0.84	0.69
	Vertical Acceleration	0.15	0.50	1.76	0.87	2.43	3.20	2.37	2.74
	Total	4.59	5.03	9.75	9.93	17.81	20.66	21.47	21.69
Outer face Tension at T	Static	6.73	6.73	5.24	5.21	10.30	10.28	11.25	11.25
	Horizontal Acceleration	0.41	0.52	1.08	0.21	0.68	0.11	0.92	0.93
	Vertical Acceleration	0.46	0.95	1.08	1.21	1.58	2.41	1.73	2.36
	Total	7.60	8.20	7.40	6.63	12.56	12.80	13.90	14.54
Inner face Compression at C	Static	5.40	4.57	8.03	7.50	18.16	15.20	24.70	24.70
	Horizontal Acceleration	0.92	1.88	2.03	6.90	0.86	9.17	1.35	1.52
	Vertical Acceleration	0.23	0.65	2.17	2.05	3.20	3.48	3.30	3.83
	Total	6.55	7.10	12.23	16.45	22.22	27.85	29.35	30.05
Inner face Tension at T	Static	8.90	8.90	9.02	3.21	15.99	8.81	16.75	14.00
	Horizontal Acceleration	1.30	1.08	0.54	14.90	0.78	18.93	2.34	7.64
	Vertical Acceleration	0.57	1.46	1.76	0.53	2.36	1.60	1.31	2.80
	Total	10.77	11.34	11.32	18.64	19.13	29.34	20.40	24.44

Table 3. (Cont'd)

Load Case		H-d-I	H-d-D	H-2d-I	H-2d-D	S-d-I	S-2d-I
Outer face Compression at C	Static	3.67	3.67	6.60	6.60	1.85	12.88
	Horizontal Acceleration	0.03	0.13	0.10	0.17	7.57	4.55
	Vertical Acceleration	0.57	0.96	0.83	1.42	1.53	3.57
	Total	4.27	4.76	7.53	8.19	10.95	21.00
Outer face Tension at T	Static	1.21	1.20	1.47	1.16	4.50	5.50
	Horizontal Acceleration	0.11	0.51	0.12	0.28	6.33	17.90
	Vertical Acceleration	0.24	0.44	0.27	0.75	1.55	1.93
	Total	1.56	2.15	1.86	2.19	12.38	25.33
Inner face Compression at C	Static	5.38	5.38	10.56	10.56	3.91	15.93
	Horizontal Acceleration	0.65	1.12	0.88	1.29	7.51	5.00
	Vertical Acceleration	0.88	1.20	1.38	1.97	1.11	4.60
	Total	6.91	7.70	12.82	13.82	12.53	25.53
Inner face Tension at T	Static	4.68	4.68	6.93	6.93	5.83	14.48
	Horizontal Acceleration	0.13	0.20	0.23	0.44	6.45	14.33
	Vertical Acceleration	0.82	1.14	1.00	1.60	2.50	3.85
	Total	5.63	6.02	8.16	8.97	14.78	32.66

Table 4. Non-dimensional Maximum Static and Total Stresses, and Dynamic Load Factors (DLF) for Various Load Cases

Load Cases		M-0-I	M-0-D	M-d-I	M-d-D	M-2d-I	M-2d-D	M-4d-I	M-4d-D
Outer face	Compression								
	Maximum Total Stress	4.59	5.03	9.75	9.93	17.81	20.66	21.47	21.69
	Maximum Static Stress	3.64	3.64	7.44	7.44	14.97	14.97	18.22	18.22
	DLF	1.26	1.38	1.31	1.33	1.19	1.38	1.18	1.19
Outer face	Tensile								
	Maximum Total Stress	7.60	8.20	7.40	6.63	12.56	12.80	13.90	14.54
	Maximum Static Stress	6.72	6.72	5.24	5.24	10.32	10.32	11.54	11.54
	DLF	1.13	1.22	1.41	1.26	1.22	1.24	1.20	1.26
Inner face	Compression								
	Maximum Total Stress	6.55	7.10	12.23	16.45	22.22	27.85	29.35	30.05
	Maximum Static Stress	5.42	5.42	8.22	8.22	18.32	18.32	24.66	24.66
	DLF	1.21	1.31	1.51	2.01	1.21	1.52	1.19	1.22
Inner face	Tensile								
	Maximum Total Stress	10.77	11.34	11.32	18.64	19.13	29.34	20.40	24.44
	Maximum Static Stress	9.13	9.13	8.88	8.88	15.94	15.94	16.74	16.74
	DLF	1.18	1.25	1.27	2.11	1.20	1.84	1.22	1.46

Table 4, (Cont'd)

Load Cases		H-d-I	H-d-D	H-2d-I	H-2d-D	S-d-I	S-2d-I
Outer face	Compression	4.27	4.76	7.53	8.19	10.95	21.00
		3.66	3.66	6.61	6.61	4.56	14.58
	DLF	1.16	1.31	1.14	1.24	2.41	1.44
Outer face	Tensile	1.56	2.15	1.86	2.19	12.38	25.33
		1.20	1.20	1.46	1.46	4.51	11.51
	DLF	1.29	1.81	1.27	1.51	2.75	2.21
Inner face	Compression	6.91	7.70	12.82	13.82	12.53	25.53
		5.51	5.51	10.61	10.61	4.43	15.95
	DLF	1.26	1.40	1.21	1.31	2.82	1.61
Inner face	Tensile	5.63	6.02	8.16	8.97	14.78	32.66
		4.67	4.67	6.92	6.92	6.10	16.83
	DLF	1.20	1.29	1.18	1.30	2.42	1.94

that the maximum non-dimensional tangential stress increases with an increase in the width of the load applied at the ground surface. When the load width is increased from d to $2d$, the compressive stress increases by 81% and the tensile stress by 71%. However, the respective increases in the maximum stress for compression and tension are 32% and 6% when the load width is increased from $2d$ to $4d$. Thus, it can be seen that the rate of increase in the maximum pipe stress diminishes with an increase in the width of the surface load. Consequently, the effect of an increase in the load width larger than $4d$ may be unimportant. The dynamic load factors, on the other hand, tend to decrease only slightly with an increase in the load width from d to $4d$.

The values of maximum stresses and dynamic load factors for the above mentioned load cases for the outer face show similar trend.

The given soil-pipe system was also analyzed for the medium soil with only the soil overburden without any superimposed surface loads. Static stresses, in this case, are in a direction opposite to that found for the surface superimposed loads. This is evident when Figures 12 and 13 are compared with Figures 16 and 17, respectively. The maximum total compressive stress at the inner face of the pipe due to the overburden alone is 6.55, whereas the corresponding stress for a load width of d at the ground surface is 12.23. The respective dynamic load factors are 1.21 and 1.51. The maximum tensile stress at the inner face of the pipe due to the soil overburden alone, on the other hand, is 10.77. The corresponding maximum tensile stress for the case with a surface load width of d is found to be 11.30. The respective dynamic load factors calculated from the tensile stresses are 1.18 and 1.27. It is evident from these values that the maximum stresses and dynamic

load factors are lower for those cases where no superimposed surface loads are applied. Inspection of the values in Tables 3 and 4 indicates that similar trends also exist at the outer face of the pipe.

Analyses with strain-independent hard soil were carried out for uniform surface load widths of d and $2d$. Plots of non-dimensional stresses for these cases are shown in Figures 28, 29, 32 and 33. Maximum total compressive stress at the inner face of the pipe for this soil increases from 6.91 to 12.82 (an increase of 85%) when the load width is increased from d to $2d$. However, the dynamic load factor reduces from 1.26 to 1.21 with an increase in the load width. Maximum tensile stress at this face, on the other hand, increases by 45% to 8.16 with an increase in the load width from d to $2d$. The respective dynamic load factors are 1.20 and 1.18. Although the magnitudes of the maximum stresses and dynamic load factors at the outer face of the pipe are different than those at the inner face, trends of an increase in the value of the stress and decrease in the dynamic load factor with an increase in the load width remain the same for both faces.

For the analyses of the soil-pipe system performed with the soft soil with strain-independent material properties and superimposed surface load widths of d and $2d$, the results are shown in Figures 36, 37, 38, and 39. At the inner face, the maximum compressive stress increases from 12.53 to 25.53 with an increase in the load width from d to $2d$ yielding a stress increase of 105%. The corresponding dynamic load factor, on the other hand, reduces from 2.82 to 1.61. The maximum tensile stresses at this face for load widths d and $2d$ are 14.78 and 32.66, respectively, indicating an increase of 121%. The respective dynamic load factors are 2.42 and 1.94. Similar increases in stress

and decreases in dynamic load factors due to an increase in the load width are observed for the outer face of the pipe.

From the results given above for the three kinds of soils using strain-independent properties, it can be stated that the maximum stress in the pipe increases as the width of the superimposed surface load is increased. This increase is substantial for all soils, especially when the load width is increased from d to $2d$, with the percentage increase for the soft soil being somewhat larger. The dynamic load factors, which give increase in the stress level due to seismic excitation over and above the existing state of stress, tend to decrease with an increase in the load width. This reduction is significant only when the pipe is surrounded by a soft soil.

Strain-Compatible Soil Properties

As indicated earlier, load widths of d , $2d$ and $4d$ were also utilized in the analyses of soil-pipe system with medium soil using strain-compatible material properties. Total stresses in the pipe due to the resulting load cases (i.e., $M-d-D$, $M-2d-D$ and $M-4d-D$) are plotted in a non-dimensional form and are shown in Figures 18, 19, 22, 23, 26 and 27. The values of maximum stresses and dynamic load factors for the corresponding load cases are given in Tables 3 and 4, respectively.

In order to evaluate the effect of a variation in the width of the superimposed load on the maximum pipe stresses in the case of strain-compatible soil properties with medium soil, the values of the maximum compressive and tensile stresses are examined at the inner and outer faces of the pipe. The maximum compressive stresses at the inner face of the pipe for load widths d , $2d$, and $4d$ are 16.45, 27.85, and 30.05, respectively, and the respective dynamic load factors are 2.01, 1.52, and 1.22.

The maximum tensile stresses at the inner face, on the other hand, are 18.64, 29.34, and 24.44 for these loads with the corresponding dynamic load factors of 2.11, 1.84 and 1.46. These results for the strain-compatible soil appear to be very similar to those obtained for the corresponding analyses using strain-independent soil properties. There is a 70% increase in the maximum compressive stress and 58% increase in the maximum tensile stress when the load width is increased from d to $2d$. For a further increase in the load width from $2d$ to $4d$, the maximum compressive stress increases by 8% while the maximum tensile stress reduces by 17%. The values of dynamic load factors tend to decrease with an increase in the width of the superimposed surface load. Similar trends can also be observed for the stresses at the outer face.

As in the case of strain-independent soil properties, one case without any superimposed surface load was also analyzed for strain-compatible soil properties using the medium soil. The total stresses for this case (i.e., M-0-D) are shown in Figures 14 and 15, and the corresponding maximum total stresses and dynamic load factors are given in Tables 3 and 4, respectively. It can be seen that the maximum stresses and dynamic load factors are lower in this case than the corresponding quantities with the superimposed loads. This behavior is similar to that which was observed for the corresponding case with strain-independent soil properties.

The influence of the superimposed surface load width on pipe stresses for hard soil using strain-compatible properties is considered for load widths d and $2d$ only. The resulting stresses are plotted as shown in Figures 30, 31, 34 and 35, and the corresponding maximum stresses and dynamic load factors are again given in Tables 3 and 4, respectively.

From the values in Table 3, it can be seen that the maximum total compressive stress at the inner face of the pipe increases from 7.70 to 13.82 (an increase of 80 %) as the load width is increased from d to $2d$. The dynamic load factor, on the other hand, decreases from 1.40 to 1.31. The maximum tensile stress at the inner face also undergoes a similar increase, i.e., from 6.02 to 8.97 (an increase of 49 %), with the corresponding increase in the load width. The dynamic load factor for tensile stress, on the other hand, does not experience any appreciable change due to an increase in the load width in this case (e.g., 1.29 vs. 1.30). Similar increase in the maximum stress and decrease in the dynamic load factor can be observed at the outer face of the pipe.

As indicated earlier under General Considerations, no analyses using strain-compatible soft soil were performed because of the unrealistic values of the resulting shear modulus for soil.

From the results presented and discussed in this section for strain-compatible soil, it can be concluded that the maximum stresses in the pipe increase substantially with an increase in the width of the superimposed surface load. This stress increase occurs primarily as the load width increases from d to $2d$. A further increase of load width from $2d$ to $4d$ does not increase the stresses significantly. The dynamic load factors generally tend to decrease with an increase in the width of the superimposed surface load.

These observations from the analyses with strain-compatible soil are similar to those that were made from the analyses with strain-independent soil.

Comparison of Stresses due to Strain-Independent
and Strain-Compatible Soil Properties

As analyses with strain-compatible soil properties have been performed for medium and hard soils only, results of these two cases are compared. The values of maximum stresses and dynamic load factors for each case are given in Tables 3 and 4, respectively.

Medium Soil

The tangential stress distribution around the pipe for various load widths is shown in Figures 16 through 27.

For strain-independent soil properties, the maximum compressive stresses at the inner face of the pipe for surface load widths of d , $2d$, and $4d$ are 12.23, 22.22 and 29.35, respectively. These stresses increase by 35%, 25%, and 2%, respectively, to 16.45, 27.85, and 30.05 when strain-compatible soil properties are used. The corresponding dynamic load factors for the strain-independent soil are 1.51, 1.21, and 1.19 which increase to 2.01, 1.52, and 1.22, respectively, for the strain-compatible soil. Similarly, the maximum tensile stresses at the inner face of the pipe due to load widths d , $2d$ and $4d$ increase by 65%, 54%, and 20%, respectively, when strain-compatible instead of strain-independent soil properties are utilized. The dynamic load factors based on the maximum tensile stresses at the inner face of the pipe also become larger with the use of strain-compatible soil properties. The maximum stresses and dynamic load factors at the outer face of the pipe generally tend to behave in a fashion similar to that at the inner face.

From the results given above for the medium soil, it is obvious that for all load widths the maximum total stresses in the pipe

obtained with strain-compatible soil properties are higher than those obtained with strain-independent soil properties. This increase, which is largest when the surface load width is d , gradually reduces as the load width increases to $4d$. The dynamic load factors are also generally larger for strain-compatible soil properties.

Hard Soil

Analyses with strain-compatible hard soil were carried out for load widths of d and $2d$ only. The resulting total stresses around the pipe for strain-independent and strain-compatible soil properties for these two load widths are shown in Figures 28 through 35.

The maximum compressive stresses at the inner face of the pipe for surface load widths of d and $2d$ are 6.91 and 12.83 if strain-independent hard soil is utilized in the analyses. These stresses increase by 11% and 8%, respectively, for the strain-compatible soil. A similar increase in the maximum stresses and dynamic load factors is also observed for the tensile stresses at the inner face. The maximum stresses as well as the dynamic load factors at the outer face follow a trend similar to the one at the inner face.

The results obtained using the strain-independent and strain-compatible soil properties are very similar for medium and hard soils. The non-dimensional maximum total stresses in the pipe for each soil are found to be higher when strain-compatible rather than strain-independent soil properties are used in the analysis. However, this difference is larger for the medium soil and smaller for the hard soil. In addition, this difference reduces as the surface load width increases. Also, the dynamic load factors in the case of strain-compatible soils are larger.

Effect of Soil Stiffness on Pipe Stresses

Once again, as superimposed surface load widths of d and $2d$ only have been used in the analyses with soft and hard soils, results for only two load widths are compared. In addition, as no analyses have been carried out using strain-compatible soil properties for the soft soil, comparisons are made only between the hard and medium soils in this case. However, the results of all three soils, i.e., hard, medium and soft, are compared for cases involving strain-independent soil properties. The maximum total stresses in the pipe and the dynamic load factors will again be taken from Tables 3 and 4, respectively, for comparison purposes.

Strain-Independent Soil Properties

For a load width of d , the non-dimensional maximum total compressive stresses at the inner face of the pipe for hard, medium, and soft soils are 6.91, 12.23, and 12.53, respectively. The corresponding dynamic load factors are 1.26, 1.51, and 2.82. The maximum tensile stresses in the pipe at the inner face for these soils, on the other hand, are 5.63, 11.30, and 14.78, with the corresponding dynamic load factors as 1.20, 1.27, and 2.42. It can be seen that as the stiffness of the soil decreases, the maximum non-dimensional stress in the pipe as well as the dynamic load factor increase. This trend is also observed at the outer face of the pipe.

When the superimposed surface load width is increased to $2d$ for the three soils, trends similar to those established for the load width d are again observed. In this case, for example, the maximum non-dimensional total compressive stresses at the inner face of the pipe for hard,

medium, and soft soil are 12.82, 22.22, and 25.53, respectively. The respective dynamic load factors are found to be 1.21, 1.21, and 1.61.

Strain-Compatible Soil Properties

If strain-compatible soil properties are used, the maximum total compressive stresses at the inner face of the pipe for load width d for hard and medium soils are 7.70 and 16.45, respectively. The corresponding dynamic load factors are 1.40 and 2.01. The respective tensile stresses at the inner face of the pipe, on the other hand, are 6.02 and 18.64 with the corresponding dynamic load factors as 1.29 and 2.11. As in the case of strain-independent soil properties, it is evident from these results that the maximum non-dimensional stresses as well as the dynamic load factors are higher for the medium soil than the hard soil.

Similar trends for the maximum stresses and dynamic load factors are observed when the load width is increased to 2d.

From the results given above for various soils with different stiffnesses, it can be concluded that the maximum non-dimensional total stresses in the buried pipe increase as the stiffness of the soil decreases. The corresponding dynamic load factors also increase with a decrease in the soil stiffness and can be as high as 2.82 for soft soils.

CONCLUSIONS AND SUGGESTIONS FOR FUTURE RESEARCH

Conclusions

Underground buried pipe as shown in Figure 3 was analyzed when subjected to seismic excitation for three different kinds of soils and various loading conditions using strain-compatible and strain-independent soil properties as shown in Table 1. Static and dynamic stresses for all the load cases along with the corresponding dynamic load factors are obtained at the outer and inner faces of the pipe. In the preceding chapter, effects of the variations in some parameters on the pipe stresses and dynamic load factors were established. Conclusions based on these results are presented in this chapter. Although these conclusions are based on the results of limited analyses performed on pipes buried at a fixed shallow depth, and subjected to a hypothetical earthquake excitation, it is expected that these conclusions could also be applicable to pipes buried at somewhat larger depths and subjected to other earthquake loads.

1. The dynamic load factor, which gives the increase in the stress level due to seismic excitation over and above the existing state of stress due to static loads, is found to be as high as 2.82 if the pipe is buried in a soft soil. This factor decreases to a maximum of 2.10 for the medium soil and 1.40 for the hard soil. Thus, it is clear that, in the event of an earthquake, the stiffness of the soil surrounding a buried pipe does have a large influence on the behavior of the buried pipe. After reviewing the damage data from various earthquakes, Kachadoorian (7) came to a similar conclusion

that the damage in a buried pipe is inversely proportional to the soil stiffness.

From the values of the dynamic load factors given above, as well as those discussed earlier, it must be concluded, therefore, that in seismic zones the stress estimates based on static analyses alone could be very erroneous. Consequently, dynamic analyses must be carried out, especially if the pipe in question is subjected to a superimposed surface load and is buried in a soft or medium soil at a shallow depth.

2. It has been shown that the magnitudes of the total stresses and dynamic load factors are higher, in general, if strain-compatible instead of strain-independent soil properties are used in the analyses. However, as the increase due to the use of strain-compatible soil properties is fairly small (approximately 8-10%) for the hard soil, computationally expensive iterative procedure can be avoided by using strain-independent soil properties in this case without compromising accuracy. Nevertheless, the use of strain-compatible soil properties is recommended for analyses with the medium soil where an increase of up to 65% in stresses and dynamic load factors is observed. It may also be reiterated here that most of the medium soils (i.e., coarse sands) do exhibit strain-compatible properties as shown in Figures 6 and 7.

3. It is observed that, irrespective of the type of soil surrounding a buried pipe, the total stresses in the pipe increase as the width of the uniform superimposed surface load increases. The increase in the total maximum stress is about 80-100% when the load width increases from d to $2d$ and only a few percent when the load width increases

from 2d to 4d. One can conclude, therefore, that the total stresses in a buried pipe increase asymptotically with an increase in the width of the superimposed surface load. The dynamic load factors, on the other hand, generally show a decreasing trend with an increase in the load width.

Suggestions for Future Research

Although a great deal of insight has been obtained in this study concerning the load transfer on shallow buried rigid pipes due to seismic effects, the conclusions given in the previous section are based on the results of analyses in which many idealizations and assumptions have been made. Before these conclusions can be assumed to be generally acceptable for other similar cases, further research is necessary. Some of the pertinent points that need further investigation may be described as follows:

1. In the static and dynamic analyses performed in this study, it was assumed that the loading system is sufficiently long and plane strain condition exists. The surface loads may often be concentrated, however, and the response of a buried pipe, in this case, may or may not necessarily be similar to that described in this study. The effect of point loading on the maximum stresses in a buried pipe should, therefore, be investigated.

2. No consideration has been given in the analyses to the steel reinforcement that generally exists in a concrete pipe (or a tunnel lining). Analyses in which the steel reinforcement has been modelled should also be performed for some load cases to ascertain whether the results without the inclusion of steel reinforcement are valid.

3. The magnitudes of stresses that are induced in a buried pipe due to soil overburden and superimposed surface loads naturally depend upon the depth of burial of a pipe. The relative contribution to the total stresses in a pipe from the soil overburden and superimposed surface loads will change with the depth of the pipe, and may be different for the static and dynamic loads. As a soil overburden of one pipe diameter only has been considered in the analyses presented in this study, additional analyses with other depths must be performed before the values of the dynamic load factors given in Table 4 can be generally accepted for other depths.

Similarly, analyses with locations of the rigid base at depths other than d below the pipe should also be carried out.

4. The conclusions given in the previous section were based on the utilization of a hypothetical earthquake shown in Figure 9. Different set of conclusions may be anticipated if the soil-pipe system is subjected to different earthquake excitations, for example, those due to El Centro or 1971 San Fernando Valley earthquakes. Such analyses should, therefore, be performed depending upon the history of earthquakes in a given region.

5. In actual field conditions, it is not uncommon to encounter various horizontal layers of soil with different material properties. Hence, it would be most appropriate to further investigate the pipe behavior under these conditions. Moreover, since a trench is usually excavated before a pipe is laid, which is then surrounded by a layer of soft material, analyses must be carried out with these material properties to assess their influence on the maximum pipe stresses and dynamic load factors.

6. The effect of slippage at the pipe-soil interface as well as the possible inability of tensile stress transfer between the pipe and soil should be investigated.

LIST OF REFERENCES

1. Wang, L. R. L. and O'Rourke, M. J., "Overview of Buried Pipelines Under Seismic Loading," Journal of the Technical Councils of ASCE, ASCE, Vol. 104, No. TC1, 1978, pp. 121-130.
2. Duke, C. M., et al., "Research Needs in Lifeline Earthquake Engineering," Journal of the Technical Councils of ASCE, ASCE, Vol. 105, No. TC2, 1979, pp. 343-362.
3. Wang, L. R. L. and O'Rourke, M. J., "State of the Art of Buried Lifeline Earthquake Engineering," Proceedings of Current State of Knowledge of Lifeline Earthquake Engineering, ASCE, Los Angeles, Calif., 1977, pp. 252-266.
4. Duke, C. M. and Moran, D. F., "Guidelines for Evaluation of Lifeline Earthquake Engineering," Proceedings of U.S. National Conference on Earthquake Engineering, Ann Arbor, Mich., EERI, 1975, pp. 367-376.
5. Kubo, K., "Behavior of Underground Waterpipes During an Earthquake," Proceedings of the Fifth World Conference on Earthquake Engineering, International Association of Earthquake Engineering, Rome, Italy, 1974, pp. 569-578.
6. Ford, D. B., "Design Considerations for Underground Pipelines in Geologically Hazardous Areas," Cast Iron Pipe News, Spring/Summer, 1975, pp. 13-22.
7. Kachadoorian, R., "Earthquake: Correlation Between Pipeline Damage and Geological Environment," Journal of the American Water Works Association, Vol. 68, March 1976, pp. 165-167.
8. Ariman, T. and Muleski, G. E., "A Review of the Response of Buried Pipelines Under Seismic Excitations," The Third National Congress on Pressure Vessels and Piping, San Francisco, Calif., June 25-29, 1979, pp. 1-29.
9. Anand, S. C., "Stress Distribution Around Shallow Buried Rigid Pipes," Journal of the Structural Division, ASCE, Vol. 100, No. ST1, 1974, pp. 161-174.
10. Reyes, S. F. and Deere, D. U., "Elastic-Plastic Analysis of Underground Openings by the Finite Element Method," Proceedings, International Society of Rock Mechanics, Lisbon, 1966, pp. 477-483.
11. Anand, S. C., and Altman, J. C., "An Inelastic Soil-Structure Interaction Problem," A paper presented at the ASCE National and Environmental Engineering Meeting, New York, N.Y. Oct. 29 - Nov. 1, 1973.

12. Shen, G. Y., "Strength of Shallow Buried Concrete Pipes," A Thesis submitted to the Department of Civil Engineering in Partial Fulfillment of the Requirements for the Degree of Master of Science, Clemson University, August, 1977.
13. Ghaboussi, J. and Rankin, R. E., "Tunnel Design Considerations: Analysis of Medium-Support Interaction," Final Report, FRA-ORD&D 75-24, Department of Civil Engineering, University of Illinois, 1974.
14. Anderson, J. C. and Johnston, S. B., "Seismic Behavior of Above-Ground Oil Pipelines," Earthquake Engineering and Structural Dynamics, Vol. 3, 1975, pp. 319-336.
15. Anderson, J. C. and Singh, A. K., "Seismic Response of Pipelines on Friction Supports," Journal of the Engineering Mechanics Division, ASCE, Vol. 102, No. EM2, 1976, pp. 275-291.
16. Powell, G. H., "Seismic Response Analysis of Above-Ground Pipelines," Earthquake Engineering and Structural Dynamics, Vol. 6, 1978, pp. 157-165.
17. Lysmer, J. et al., "LUSH - A Computer Program for Complex Response Analysis of Soil-Structure Systems," Report No. EERC 74-4, Earthquake Engineering Research Center, University of California, Berkeley, Calif., April 1974.
18. Leonard, G. A., Foundation Engineering, McGraw-Hill, New York, 1962.
19. Barkan, D. D., Dynamics of Bases and Foundations, Translated from Russian by Drashevskaya, L. Translation edited by Tschebotarioff, G. P., McGraw-Hill, New York, 1962.
20. Desai, C. S. and Abel, J. F., Introduction to the Finite Element Method, Van Nostrand Reinhold Co., New York, 1970.
21. Seed, H. B., Lysmer, J. and Hwang, R., "Soil-Structure Interaction Analyses for Seismic Response," Journal of the Geotechnical Engineering Division, ASCE, Vol. 101, No. GT5, May 1975.
22. Seed, H. B. and Idriss, I. M., "Influence of Soil Conditions on Ground Motions During Earthquakes," Journal of the Soil Mechanics and Foundation Division, ASCE, Vol. 95, No. SM1, 1969, pp. 99-137.
23. Clough, R. W. and Penzien, J., Dynamics of Structures, McGraw-Hill, New York, 1974.
24. Newland, D. E., An Introduction to Random Vibrations and Spectral Analysis, Longman, London and New York, 1975.

